Chapter 1 –Introduction

Two-photon laser scanning microscopy (TPLSM) typically uses ultrashort pulsed laser sources providing high peak intensities [1], [2]. This is because the probability of two-photon absorption (TPA) depends on the square of the peak intensity [3]. Ultrashort pulsed lasers provide this high peak intensity: without ultrashort pulses, the overall average power would have to be increased to perform TPA. An undesirable consequence of increasing the average power is an increase in the likelihood of photo-bleaching [4], which may destroy the sample. Also, depending on the wavelength used, this may also contribute towards heating of the sample. These are clearly unwanted effects when imaging biological samples.

Ultrashort pulsed lasers consist of a range of wavelengths within a finite bandwidth. As this range of frequencies travels through optical elements, such as those found in a laser-scanning microscope, they become stretched in time. This results in a decrease of the peak intensity of the laser, which, in turn reduces the probability of TPA [5]. As an example of the magnitude of this problem, a 60 fs pulse at a wavelength of 800 nm with an approximate spectral bandwidth of 30 nm may increase to as much as 200 fs when propagating through a Zeiss Plan-Neo Fluor 1.4-NA oil immersion objective lens [6]. This is because an objective lens is comprised of many individual elements [7], [8], some of which vary in shape i.e. concave or convex, thickness and diameter. Consequently, when a laser beam scans across the back aperture of an objective lens during TPLSM [9] it will propagate through different thicknesses of material depending on the position of the input beam, i.e. whether it is on or off axis. As a result, it is conceivable that the probability of TPA will differ across the sample as a consequence of changes in material dispersion across the lateral direction of the objective lens stretching the ultrashort pulses by different amounts. This may affect the quality of the two-photon excited fluorescence image, as even a homogeneously fluorescing specimen may give different levels of fluorescence signal depending on the duration of the pulse at the sample plane.

This thesis will investigate the extent to which the pulse duration changes on propagation through lenses to be used in TPLSM, both on and off-axis. This includes analysis of standard objective lenses used in this technique and also a novel prototype lens intended for use in mesoscopic imaging. This will be followed by a study of dispersion compensation that could be used to reduce the pulse duration following propagation through both the standard and novel Mesolens, for improved TPLSM.

The following chapter will give an overview of optical microscopy methods and limitations, with emphasis on the role of temporal dispersion in multi-photon excitation.

1.1 Refractive index and dispersion

Dispersion occurs because the phase velocity (and the group velocity) of a wave is wavelength dependent when propagating through a dispersive medium [10]. This is often referred to as chromatic dispersion, in order to emphasize this wavelength dependent effect. Perhaps the simplest example of chromatic dispersion is a rainbow, which breaks white light up into its constituent wavelengths when propagating through a dispersive medium such as water molecules in the air. This wavelength (or frequency) dependence of the refractive index stems from the characteristic resonance frequencies at which the material absorbs the electromagnetic radiation through oscillations of bound electrons [11]. When distant from the material resonance, the Sellmeier equation becomes a good approximation to measure the refractive index of any material [11]:

$$n^2(\lambda) = 1 + \frac{B_1\lambda^2}{\lambda^2 - C_1} + \frac{B_2\lambda^2}{\lambda^2 - C_2} + \frac{B_3\lambda^3}{\lambda^2 - C_3} \quad \ldots(1)$$

where n is the refractive index, λ is the wavelength of light (μm), and $B_{1,2,3}$ and $C_{1,2,3}$ (μm^2) are experimentally determined Sellmeier coefficients. The Sellmeier coefficients are specific to the material in which the light of wavelength λ propagates, and the values can be found in most glass catalogues such as Schott [12] or in many papers for non-Schott material [13][14]. The Sellmeier relation is used to plot the dispersion curve of the refractive index as a function of wavelength for a particular material between a wavelength range of λ=365-2300 nm [15] and is used to quantify the dispersion of light within a particular transparent medium.

1.1.1 Phase velocity

Material dispersion plays an important role in ultrashort pulse propagation since the different spectral components within the pulse are travelling with varying speeds given by:

$$v_p = \frac{\omega}{k} \equiv \frac{2\pi\upsilon}{2\pi\frac{n(\lambda)}{\lambda}} \quad \ldots(2)$$

where v_p is known as the phase velocity, ω is the angular frequency, ν is the frequency and k is the wavenumber. Equation (2) simplifies to:

$$v_p = \frac{c}{n(\lambda)} \quad \ldots(3)$$

where c is the speed of light and n(λ) is the wavelength dependent refractive index. This term phase velocity refers to the velocity at which one frequency component of the wave is travelling. The phase velocity in a vacuum is equal to the speed of light since there is no interaction with any medium and is equal to the group velocity. According to Equation (3), the phase velocity will decrease when propagating through a medium since the refractive index n≥1. As shown in Equation (2), the

phase velocity has a frequency that varies, causing the phase velocity to vary and the medium is therefore termed a dispersive medium.

1.1.2 Group velocity dispersion

As mentioned, the phase velocity is the speed of one individual frequency component of a wave, which can be seen below. As a result of each of these frequency components travelling at a different phase velocity through a material it causes the overall packet to travel at the group velocity.

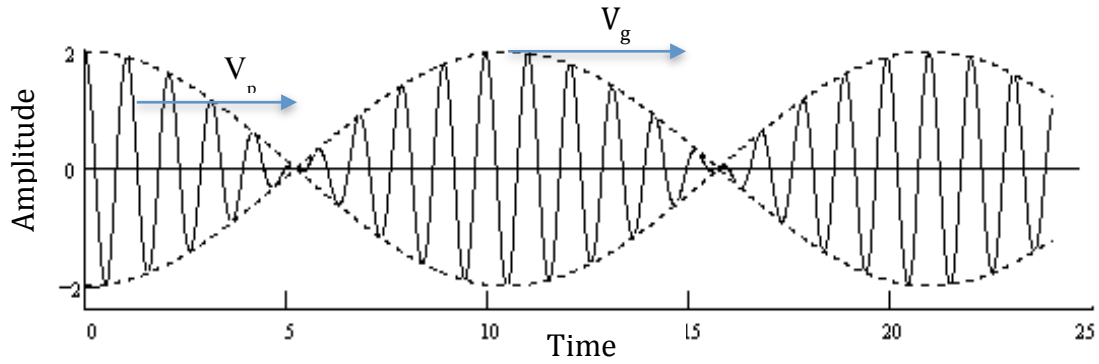

Figure 1 - Schematic diagram displaying the phase (V_p) and group velocity (V_g) of a wave.

The group velocity can be calculated by differentiating the frequency of the wave with respect to the wavenumber as shown below:

$$v_g = \frac{\partial \omega}{\partial k} \quad \text{...(4)}$$

This equation can also be written as a function of the wavelength dependent refractive index to become [16]:

$$v_g = c\left(n(\lambda) - \lambda \frac{dn}{d\lambda}\right)^{-1} \quad \text{...(5)}$$

where $n_g(\lambda)$ is the group refractive index [17]. The group velocity dispersion (GVD) is the variation of the group velocity as a function of wavelength. Equation (6) shows that the GVD is frequency dependent [10].

$$GVD \equiv \beta_2 = \frac{\partial}{\partial \omega}\frac{1}{v_g} = \frac{\partial}{\partial \omega}\left(\frac{\partial k}{\partial \omega}\right) = \frac{\partial^2 k}{\partial \omega^2} \quad \ldots(6)$$

Equation (6) can also be written as a function of the wavelength dependent refractive index thus:

$$\beta_2 = \frac{\lambda_0^3}{2\pi c^2}\frac{d^2 n}{d\lambda_0^2} \quad \ldots(7)$$

where λ_o is the central wavelength of the incident beam and the term $\frac{d^2 n}{d\lambda_0^2}$ is the second derivative of the refractive index with respect to wavelength [16]. Another useful measure of material dispersion in relation to the refractive index was introduced by Ernst Abbe and is therefore called the Abbe number which is given by Equation (8) [18]:

$$V = \frac{n_d - 1}{n_F - n_C} \quad \ldots(8)$$

where n_d, n_f and n_c are the refractive indices of a material at the wavelengths of the d, F and C Fraunhofer spectral lines. These wavelengths are 587.6 nm, 486.1 nm and 656.3 nm respectively. High material dispersion is represented by a low Abbe number and vice versa.

GVD can be normal or anomalous, which refers to positive and negative dispersion respectively. This becomes useful when utilizing compensation techniques, which will

be mentioned later in this chapter. Figure 2 shows how the refractive index, the group index and the dispersion parameter change as a function of wavelength for BK7, which is a common material for optical components.

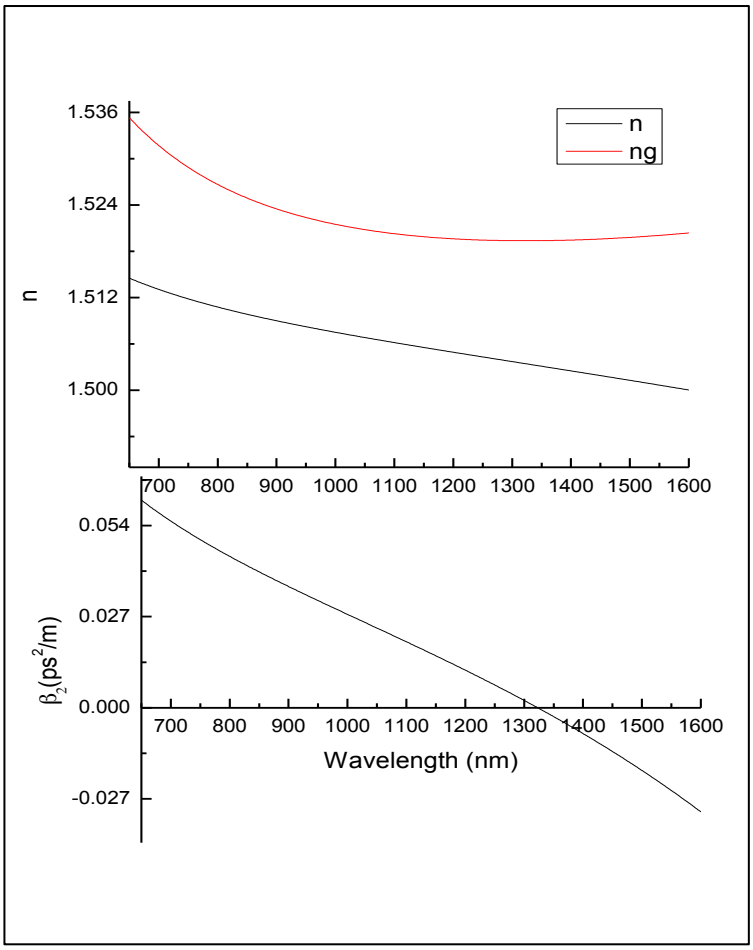

Figure 2 - Plot of the refractive index (n), the group index (ng) and the dispersion parameter (β_2), as a function of wavelength between a wavelength range of 650-1600 nm for BK7[19].

1.1.3 Temporal dispersion

This frequency dependence of GVD, shown in Equation (6), also has a significant effect on the duration of ultrashort pulses since each pulse contains a range of frequencies within a bandwidth, each of which will be affected by GVD by a different quantity. As a result, a pulse will propagate through a medium with different frequency components within the bandwidth all travelling at slightly different speeds,

where the red components are travelling faster than the blue (normal dispersion) or the blue travels faster than the red (anomalous dispersion). The shape of the pulse is then broadened by this difference in velocities, known as temporal dispersion. As will be shown, the shorter pulse durations have a much more significant increase than the longer pulses when propagating through a series of dispersive optical elements which can be problematic when using sub-100 fs ultrashort pulses during TPLSM.

1.2 Dispersion in laser scanning microscopy

As described, dispersion has an overall effect on the duration of ultrashort pulses, which becomes problematic for laser scanning microscopy where ultrashort pulses are preferred for a higher probability of TPA [20]. The lower pulse durations require a higher input power from the laser to achieve TPA that in turn causes heating of the sample, which is an undesired effect for any biological samples. Many studies have been carried out to try and overcome this or to study the magnitude of the problem and the effect this has on fluorescent imaging.

1.2.1 Overview of laser scanning microscopy

Laser scanning microscopy involves raster scanning a sample with a diffraction-limited spot of laser light, where the diffraction limit can be found by Equation (8) [21].

$$r_{lat} = \frac{0.61\lambda}{NA} \quad ...(8)$$

where λ is the wavelength (m) and NA is the numerical aperture of the objective lens.

The scanning takes place by either moving the sample or the laser beam to form a complete image of the whole sample [22]. As the laser beam is focused into the sample it excites fluorescence, which is detected by a photodetector converting light

into current by the photoelectric effect [23]. Computer analysis then converts the intensity of the fluorescence into an image of the sample by constructing an image of the sample pixel by pixel to create clear optical sections. 3D images can then be reconstructed by imaging the sample at different depths and combining a multitude of 2D images using computer software [24]. This explanation is generalized to the whole area of laser microscopy, however there are several different branches such as confocal laser scanning microscopy (CLSM) and two-photon laser scanning microscopy (TPLSM), both of which will be discussed in detail.

1.2.1.1 Confocal microscopy

Since the invention of the first confocal microscope it has become a very important tool in the microscopy field because of its innovative ability to create three-dimensional images of samples between approximately 10-200 µm thick depending on the sample tissue [25]. It illuminates the dyed specimen point by point and involves limiting the light detection by two pinholes, one of which is located on the sample plane in front of the detector and the other in front of the illuminating laser [21]. In doing so, it is able to reject light that is above or below the confocal range (Figure 3).

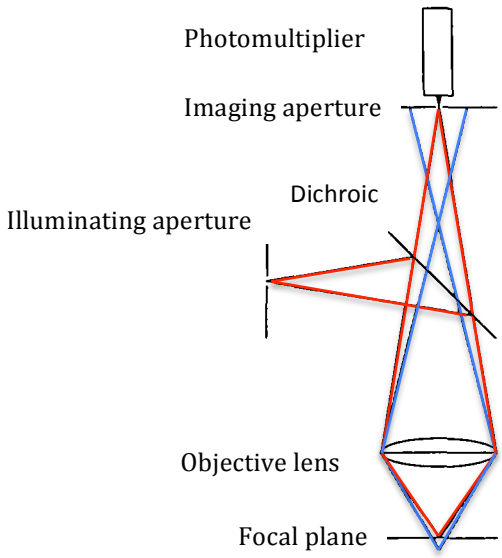

Figure 3 - The principle of CLSM, which displays the path that the rejected out of focus light (blue) takes by use of two pinhole apertures [26]**. The red and blue are not an indication of wavelength.**

Modern confocal microscopes use a continuous wave (cw) laser at the appropriate wavelength for the light source to instigate a process known as fluorescence [24], which absorbs the incident light and subsequently emits light of a different wavelength. The emitted light is collected using a photomultiplier tube or other photodetector, as mentioned previously. During the imaging process the light from the source (of shorter wavelength) reflects off a dichroic mirror to a pair of scanning mirrors, one of which scans horizontally and the other vertically. These mirrors work together to scan the laser across the back of the objective lens, which focuses onto different points of the sample. In doing so, it excites the dye to emit fluorescent light that is then able to travel back through the optical path, through the dichroic mirror onto the photo-multiplier tube (PMT). The detector is attached to a computer, which is able to construct 3D images, as mentioned previously.

Many studies use this method of microscopy including, for example, [27-29] since it has several advantages such as an improved signal to noise ratio, increase in resolution and it reduces the blurring caused by light scattering through the sample [21].

1.2.1.2 Multi-photon microscopy

Multi-photon microscopy, which is a non-linear process, is a technique used for deep imaging, the preferred choice for highly scattering samples including biological tissue. The reason being that the high photon concentration, which is required for excitation, only occurs at the focal point and therefore has the ability of excluding fluorescence that is not at the focal point [30]. Multi-photon microscopy (often referred two as two-photon microscopy although three-photon microscopy also exists [31]) uses pulsed lasers at a longer wavelength, typically around the infrared (IR) end of the spectrum and excites the fluorophore by a process known as two-photon absorption (TPA) in a non-linear fashion. Absorbing two longer wavelength photons excites the fluorophore into the excited state and is then spontaneously emitting one shorter wavelength photon, with the emission process similar to that for single-photon excitation as per the confocal case [30]. Just as in the case described before for CLSM the emitted light from the fluorophore is collected by a photo- detector, which then builds up an image of the entire sample of interest. An advantage of two-photon microscopy is the ability to only excite fluorescence at the focal point as opposed to one-photon excitation, which occurs all the way through the beam path (Figure 4). The reason for this being that the probability of TPA to occur is extremely low and therefore will only occur at the focal point of the beam where the photon density is at its highest [32]. Other subtle advantages include the emission of photons in the visible range, IR light having the ability to penetrate deeper into more scattering samples and is also not as phototoxic to biological samples [32].

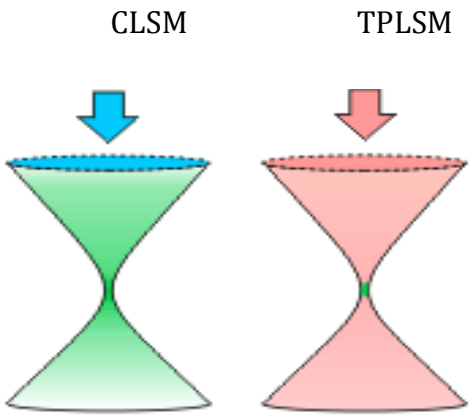

Figure 4–CLSM vs TPLSM, where the area in green for both CLSM and TPLSM is the excited fluorescence[30], [32].

As mentioned, this study is analyzing the effect of material dispersion on the duration of sub-ps pulses and since CLSM use cw lasers we will be concentrating on the effect this has on TPLSM only.

1.2.1.2.1 Lasers for multi-photon microscopy

As mentioned, multi-photon microscopy utilizes TPA, which has a low probability rate and therefore requires ultrashort pulsed lasers. As will be discussed in the proceeding sections the probability of two-photon absorption is proportional to the intensity squared (I^2) and for three-photon microscopy it is the intensity cubed (I^3) and so on [33]. In order to achieve efficient multi-photon excitation using ultrashort pulsed lasers the photons must collide with the individual molecules simultaneously. Hence the use of ultrashort pulsed lasers such as Ti:Sapphire. This laser is the most commonly used laser for multi-photon excitation [34], [35], which has a typical wavelength between approximately 710-1000 nm [36] and a typical pulse duration ($\Delta\tau$) of approximately 100-200 fs [21], [37]. To fully understand the use of the Ti:Sapphire laser several other parameters should be explored including the peak intensity (I_{peak}), the average power (P_{ave}), and the repetition rate ($\Delta\nu$). Ultimately, the aim is to increase the peak intensity since the probability of absorption is proportional to the square of the peak intensity. However certain methods of increasing the intensity (such as increasing the average power of the laser) will generate high levels of heat within the sample, which is an undesired effect when

working with cellular structures. Similarly the repetition rate is a trait that is determined by each individual laser and therefore cannot be easily altered. However simply reducing the pulse duration can make a further increase in the peak intensity, in turn causing the peak power for every emitted pulse to be significantly higher according to Equation (9).

$$P_p = \frac{P_{ave}}{\Delta\tau\Delta\upsilon} \quad \ldots(9)$$

where $\Delta\nu$ is approximately 76MHz for most commercial Ti:Sapphire lasers. As shown, reducing the pulse duration will increase the peak power of each pulse, which has a direct effect on the efficiency of TPA since it is a non-linear function of peak power [38].

1.2.2 Temporal dispersion in multi-photon microscopy

We consider first the increase in pulse duration after propagation through an optical system and its effect on the TPA probability as described by the following equation [39], [40]:

$$n_a = \frac{p_{ave}^2 \delta}{\Delta\tau\left(\Delta\upsilon\right)^2}\left(\frac{NA^2}{2\hbar c\lambda}\right)^2 \quad \ldots(10)$$

where n_a is the number of photons absorbed per fluorescent molecule per pulse, p_{ave} is the input power (approximately in the 10s of mW region for multi-photon microscopy), δ is the TPA cross section (cm^4seconds/photon), which varies between fluorophores and wavelengths, NA is the numerical aperture of the microscope objective, c is the speed of light (ms^{-1}) and ħ is the Planck quantum of action [40](Js).

As mentioned, the input pulse duration into an optical system (such as an objective lens) can significantly increase the duration of sub-ps pulses as a result of material

dispersion and therefore significantly reduce the probability of TPA, making it difficult or impossible to obtain a contrast image of the specimen under investigation. As such, it is important to consider the pulse duration when designing a multi-photon microscope.

As shown, the excitation efficiency of TPA is highly dependent upon the pulse duration of the excitation pulse. As the pulses of laser light propagate through the microscope optics and the objective lens they become increasingly stretched, or as commonly known ''chirped'', since the different wavelengths are slowed down by varying amounts. The aim for this project is to describe the effect of material dispersion upon the pulse duration through the objective lens of a microscope. Equation (11) describes the increase in pulse duration through a length of material with an initial pulse duration τ_o assuming a Gaussian pulse [11].

$$\tau_1 = \tau_0 \sqrt{1 + \left(\frac{z}{L_D}\right)^2} \quad \ldots(11)$$

where z is the position in the material and the dispersive length (L_D) is described as:

$$L_D = \frac{\tau_0^2}{|\beta_2|} \quad \ldots(12)$$

Despite this calculation assuming a temporal Gaussian pulse, it is a good enough approximation to apply to the hyperbolic secant ($sech^2$) pulse shape which is produced by an ultrashort pulsed Ti:Sapphire laser. Further details of this are in the following chapter.

1.3 Dispersion compensation schemes to manage pulse broadening

Having demonstrated the extent to which material dispersion affects the probability of TPA we will now go on to discuss a compensation technique, which is implemented to overcome this problem. Techniques that have been studied extensively and reported studies on optical pulse compression include the use of photonic crystal fibres (PCF), diffraction gratings or prisms [11]. A few studies even use a combination of these methods to comprise a pulse compression system [41]. In this study however, the dispersion compensation will be looked at using diffraction gratings alone.

The high intensity light pulses create a local index of refraction that is higher towards the centre of the pulse and therefore results in the leading and trailing edges of the pulse to have different effects upon the frequency. The term chirp is often used to express this change in frequency, where an up-chirp defines the shift of frequency to that of higher frequencies, which is caused by the trailing edge and down-chirp describes the leading edge of the pulses shift to that of lower frequency. The principle of dispersion compensation involves stretching the initial pulse in one direction in time so that during propagation through the entire set of optical elements the trailing edge of the pulse has caught up with the leading edge and therefore having the original pulse (or compressed pulse) at the sample plane [3].

1.4 Conclusion

As shown, material dispersion plays an important role in TPLSM and consequently has an overall effect on image quality. The following chapters will determine the scale of the problem of material dispersion present in the objective lenses of any optical system by comparing experimental measurements to numerical models and in turn will be able to determine the corresponding effect this increase in pulse duration has on the probability of TPA. Pre-dispersion compensation techniques will also studied by using suitable diffraction gratings, which are capable of stretching the pulse before propagating through the objective lens. In doing so, a shorter pulse duration will cause the increase in probability of TPA which is required for efficient imaging in TPLSM.

Chapter 2 - Numerical simulation of pulse broadening in commercial microscope objective lenses: on-axis and off-axis

2.1 Introduction

As discussed in Chapter 1, one of the aims of this thesis is to understand how propagation of an ultrashort pulse compares when on and off-axis through an objective lens. This chapter focuses on deriving relationships that can be applied to any objective lens to determine the output pulse duration after propagation through a series of optical elements and applying these to two different objective lenses. One of the difficulties in understanding pulse evolution is that the properties of the individual lens elements, i.e. the thickness and material type, must be known but most commercial microscope objective lens manufacturers do not provide this information. As such, the numerical data for two generic objective lenses are used in this Chapter. These were chosen because the element details were available and the numerical aperture and magnification was similar to lenses used in TPLSM and for the experimental study that will be shown in Chapter 3. The data for these lenses is used to illustrate this method and will then be used to calculate the effect this has on TPA, both on and off axis

2.2 Theory

2.2.1 Ultrashort pulse through multiple elements

Following Agrawal [11] the theory and analysis of stretching of ultrashort pulses through multiple elements will be explored below. In doing this, we will produce an expression that can be applied to any optical lens system to determine the effect of dispersion on the output pulse duration of an optical pulse. We first consider the simple equation that determines the pulse propagation through any transparent medium, which is given by the nonlinear Schrodinger equation [11]:

$$\frac{i\partial U}{\partial z} = -\frac{1}{2}\alpha U + \frac{1}{2}\beta_2 \frac{\partial^2 U}{\partial t^2} - \gamma |U|^2 U \quad \text{...(13)}$$

where U is the amplitude of the wave, z is the position in the material, t is time, β_2 is the dispersion constant given previously in Equation (7) of Chapter 1, and γ is the constant of nonlinearity. The first term on the right hand side of the equation then describes the effect of absorption, the second term describes the effect of dispersion and finally the third term describes the effect of nonlinearity. The magnitude of each term relative to one another is important in determining how the pulse shape will behave during propagation. Since we are interested in the transmission of light in transparent optical material, the absorption term has been set to zero. If the input pulses are ultrashort, the dispersion term is dominant and the nonlinearity term can also be neglected (i.e. we set γ=0). Therefore, in order to study the effect of GVD on ultrashort pulses propagating through a linear dispersive medium the partial differential Equation (13) simplifies to:

$$\frac{i\partial U}{\partial z} = \frac{1}{2}\beta_2 \frac{\partial^2 U}{\partial t^2} \quad \text{....(14)}$$

This expression describes the temporal effect of dispersion, therefore explaining how the amplitude evolves over time in relation to β_2. By applying the Fourier transform method to Equation (14), it allows us to decompose the wave into its constituent frequencies so that instead of describing the evolution of the amplitude in relation to time it will describe how it evolves in relation to frequency. This is given by equation (15)

$$U(z,t) = \frac{1}{2\pi}\int_{-\infty}^{\infty} \tilde{U}(z,\omega)\exp(-i\omega t)\,d\omega \quad \ldots(15)$$

where ω is the frequency and $\tilde{U}(z,\omega)$ is the Fourier transform of $U(z,\tau)$. In doing so it converts the equation from time dependent into frequency dependent and by carrying out the integrals it becomes a simple differential equation:

$$i\frac{\partial \tilde{U}}{\partial z} = -\frac{1}{2}\beta_2\omega^2\tilde{U} \quad \ldots(16)$$

which have a solution of:

$$\tilde{U}(z,\omega) = \tilde{U}(0,\omega)\exp\left(\frac{i}{2}\beta_2\omega^2 z\right) \quad \ldots(17)$$

In order to calculate the effect multiple elements has on the normalized amplitude of the pulse envelope the above equation for two elements becomes:

$$\tilde{U}(z,\omega) = \tilde{U}(0,\omega)\exp\left(\frac{i}{2}\beta_{2,1}\omega^2 z_1\right)\exp\left(\frac{i}{2}\beta_{2,2}\omega^2 z_2\right) \quad \ldots(18)$$

where $\beta_{2,1}$ refers to the dispersion parameter through element 1 with length z_1 and $\beta_{2,2}$ refers to the dispersion parameter through element 2 with length z_2. This is simply the multiplication of an extra exponential term since $\tilde{U}(0,\omega)$ is simply the frequency

spectrum at z=0 which remains the same independent of the number of additional elements. This equation can be further simplified and generalized since the law of multiplying exponentials allows us to add the powers to become:

$$\tilde{U}(z,\omega) = \tilde{U}(0,\omega)\exp\left(\sum_{m=1}^{\infty}\frac{i}{2}\beta_{2,m}\omega^2 z_m\right) \quad \ldots(19)$$

which applies to an infinite number of elements with a dispersion parameter of $\beta_{2,m}$ propagating through an element of length z_m. The temporal profile of the output pulse is obtained by the Fourier Transform of Equation (19).

$$U(z,t) = \frac{1}{2\pi}\int_{-\infty}^{\infty}\tilde{U}(0,\omega)\exp\left(\sum_{m=1}^{\infty}\frac{i}{2}\beta_{2,m}\omega^2 z_m - i\omega t\right)d\omega \quad \ldots(20)$$

Equation (20) is produced by inserting Equation (19) into Equation (15) where *$\tilde{U}(0,\omega)$* is the Fourier transform of the incident field at z=0 (before propagation through any material) which is given below:

$$\tilde{U}(0,\omega) = \int_{-\infty}^{\infty}U(0,t)\exp(i\omega t)dt \quad \ldots.(21)$$

Where *$U(0, \tau)$* for a Gaussian pulse has an incident field of

$$U(0,t) = \exp\left(-\frac{t^2}{2\tau_0^2}\right) \quad \ldots(22)$$

Here, τ_o represents the half-width at 1/e intensity point [11]. Therefore by carrying out the integral in Equation (20) it gives us a solution of:

$$\tilde{U}(0,\omega)=\exp\left(-\frac{\tau_0^2\omega^2}{2}\right)\sqrt{2\pi}\tau_0 \quad \ldots(23)$$

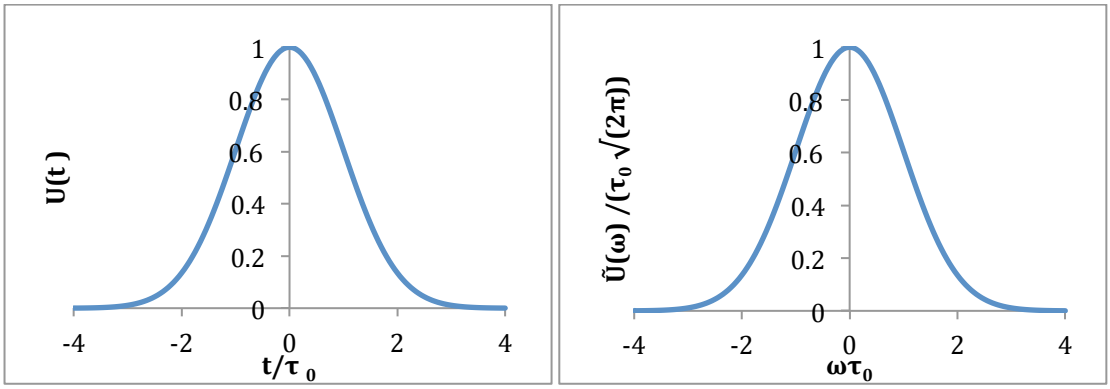

Figure 5–Plot of a Gaussian pulse in terms of time (Equation (22)) (left) and its Fourier transform in terms of frequency (Equation (23))(right).

The amplitude was calculated by combining Equations (20-22) and carrying out the integral, in doing so it provides the amplitude of the pulse envelope at any length z through the material.

$$U(z,t)=\frac{\tau_0^2}{\tau_0^2-\sum_{m=1}^{\infty}i\beta_{2,m}z_m}\exp\left(-\frac{t^2}{2\left(\tau_0^2-\sum_{m=1}^{\infty}i\beta_{2,m}z_m\right)}\right) \quad \ldots(24)$$

By multiplying the complex conjugate of the imaginary term in Equation (24) as shown below it allows us to get rid of the imaginary number on the denominator.

$$U(z,t)=\exp\left(\frac{-t^2}{2\left(\tau_0^2-\sum_{m=1}^{\infty}i\beta_{2,m}z_m\right)}\cdot\frac{\tau_0^2+\sum_{m=1}^{\infty}i\beta_{2,m}z_m}{\tau_0^2+\sum_{m=1}^{\infty}i\beta_{2,m}z_m}\right) \quad \ldots(25)$$

In doing so it provides Equation (25) where the first real term on the right hand side describes the envelope of the pulse and the second term on the right hand side shows a time-dependent imaginary term which shows the phase change moving across the pulse i.e. how chirped the pulse is.

$$U(z,t) = \exp\left(\frac{-t^2\tau_0^2 - t^2\sum_{m=1}^{\infty} i\beta_{2,m}^2 z_m^2}{2\left(\tau_0^4 + \sum_{m=1}^{\infty}\beta_{2,m}^2 z_m^2\right)}\right) \quad \ldots(26)$$

It is the amplitude of the pulse envelope that is of interest and therefore we will only consider the first term. When we compare Equation (26) to Equation (22) we find that the output pulse duration for a Gaussian pulse becomes:

$$\tau_1^2 = \frac{\tau_0^4 + \sum_{m=1}^{\infty}\beta_{2,m}^2 z_m^2}{\tau_0^2} \quad \ldots(27)$$

This therefore simplifies to become the square of the sum of the length of material divided by the dispersive length associated with each individual lens, which can be shown below:

$$\tau_1 = \tau_0\sqrt{1+\left(\sum_{m=1}^{\infty}\frac{z_m}{L_{D,m}}\right)^2} \quad \ldots(28)$$

This derivation has been carried out assuming a Gaussian pulse despite most studies involving Ti:Sapphire lasers assuming a hyperbolic secant ($sech^2$) shaped pulses [42-44] which has an incident field of the form:

$$U(0,t) = \sec h\left(\frac{t}{\tau_0}\right) \quad \text{...(29)}$$

The transmitted field can then be calculated using equations (20), (21) and (29), however the integral in equation (20) is not a simple calculation to carry out [11] and therefore the Gaussian shaped pulse is a good enough approximation since the full-width at half maximum (FWHM) of a Gaussian is related to τ_0 by:

$$\tau_{FWHM} = 2\sqrt{\ln 2}\tau_0 = 1.665\tau_0 \quad \text{...(30)}$$

which is similar to the sech^2 relation, which is related by:

$$\tau_{FWHM} = 2\ln(1+\sqrt{2})\tau_0 \approx 1.763\tau_0 \quad \text{.....(31)}$$

Having made this assumption Figure 6 below shows the broadening effect the dispersive length has on the shape of a Gaussian pulse at $z = L_D$, $2L_D$ and $4L_D$ [11], where L_D is given by equation (12) in Chapter 1.

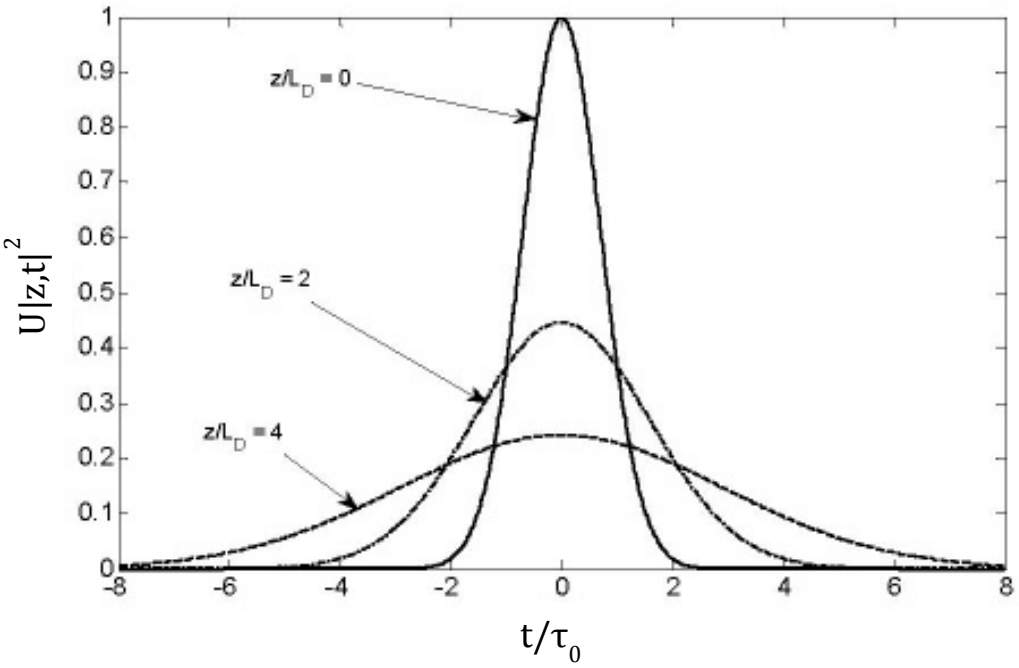

Figure 6 -The broadening caused by the dispersion on a Gaussian pulse discussed [11], [45].

Figure 6 shows that the pulse broadens further as it propagates through the material. To illustrate this, the increase in pulse duration through 100 mm of BK7 was calculated in increments of 2mm using Equation (28), using an initial pulse duration of 100 fs.

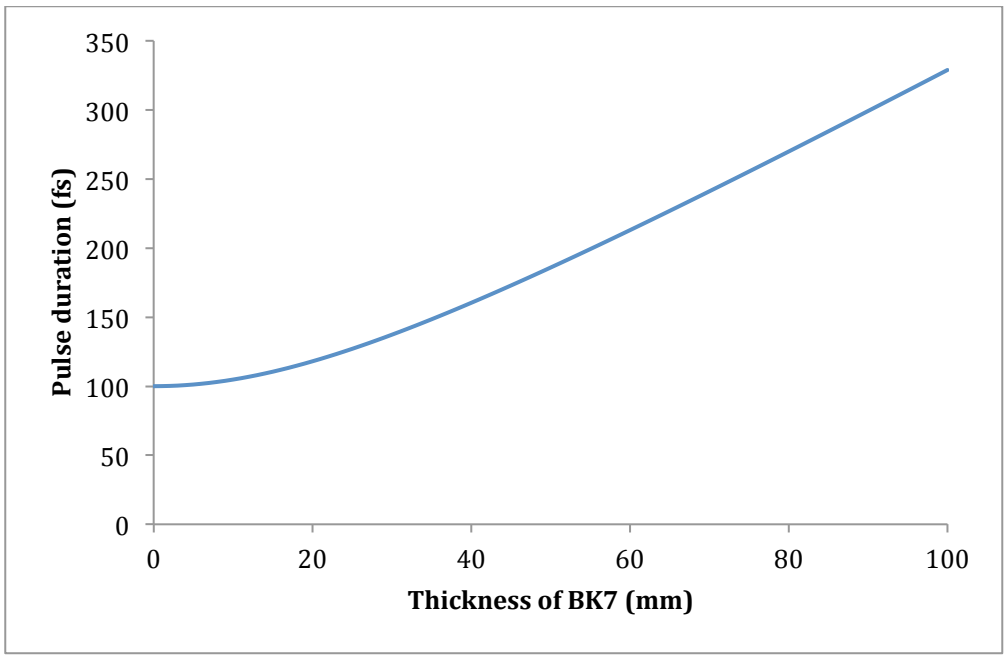

Figure 7 - Plot of the output pulse duration through increasing length of BK7. The Sellmeier coefficients were obtained from [19].

From Figure 7 it can be seen that for this particular material the pulse duration starts to increase linearly approximately around 50mm. This same asymptotic trend will be seen through any optical material, however the values may vary depending on the dispersive properties of the material and the initial parameters of the input pulse. The start of the graph can be explained by considering the frequencies within each pulse, with a bandwidth consisting of a range of pure frequencies. It takes the pulse some length of glass to completely separate the frequencies until the leading edge of the pulse is shifted down in frequency and the trailing end is shifted up at which point the pulse is becoming increasingly chirped and continues to increase in pulse duration linearly. From this graph we can then show that since the pulse duration increases linearly with thickness we can then say that for a pair of objective lenses with 10 elements in each:

$$\tau_0\sqrt{1+\sum_{i=1}^{20}\left(\frac{z_i}{L_{Di}}\right)^2}=\tau_0\sqrt{1+2\sum_{i=1}^{10}\left(\frac{z_i}{L_{Di}}\right)^2} \quad \text{....(32)}$$

This then provides us with an expression, which can be applied to determine the pulse duration after one objective lens, by measuring the initial pulse duration and the final pulse duration after propagation through a pair of identical objective lenses using an autocorrelator.

2.2.2 Numerical model for the pulse duration through an objective lens of unknown material

The previously discussed method of calculating the pulse duration is only useful when all the information is provided for the internal elements such as material name, thickness etc. However this information is not always available and therefore another method has to be implemented to provide us with the pulse duration after one objective lens of unknown internal components. As will be discussed in greater detail in the next Chapter an autocorrelator is used to measure sub-ps pulses, which will be used to measure the increase in pulse duration as a result of the material dispersion present within different objective lenses. However, the autocorrelator cannot be used immediately following propagation of the pulsed laser through one objective lens, because the beam comes to a focus and then diverges dramatically, which cannot be detected by the autocorrelator. Therefore the beam has to be collimated by placing another identical objective lens nose-to-nose with the current objective lens, separated by double the focal length until a collimated beam is produced. In doing so the autocorrelator is able to provide a value of the pulse duration after two objective lenses, which we can mathematically work back from to give a value of the output pulse duration after one objective as described in Equations (31-33) below.

In order to calculate the pulse duration after one objective lens the following method can be employed. Following Equation (32) the pulse duration after two objective lenses was found to be:

$$\tau = \tau_0 \sqrt{1 + 2\sum_{m=1}^{10}\left(\frac{z_m}{L_{D,m}}\right)^2} \quad \ldots(33)$$

By solving Equation (33) in terms of the sum of the square of the length over the dispersive length it becomes:

$$\sum_{m=1}^{10}\left(\frac{z_m}{L_{D,m}}\right)^2 = \frac{\frac{\tau^2}{\tau_0^2} - 1}{2} \quad \ldots(34)$$

The pulse duration after one objective lens can then be found by inserting the solution to Equation (34) into the equation below:

$$\tau = \tau_0 \sqrt{1 + \sum_{m=1}^{10}\left(\frac{z_m}{L_{D,m}}\right)^2} \quad \ldots(35)$$

The only difference between Equation (33) and (35) is the factor of two, which was explained earlier to be a result of the linear increase in the pulse duration through the material.

2.3 Method

The data is not available for the objective lenses used in the lab and therefore the data for two generic objective lenses of different magnification will be used throughout this Chapter, both of which were obtained from United States Patent Office [7],[8].

2.3.1 Pulse duration through a generic cytometry lens (10x/1.2 NA)

In order to mathematically determine the extent to which a pulse is stretched as a result of material dispersion the first generic objective lens was used [7], by firstly

considering an input pulse directed on-axis through the objective lens shown in Figure 8 below.

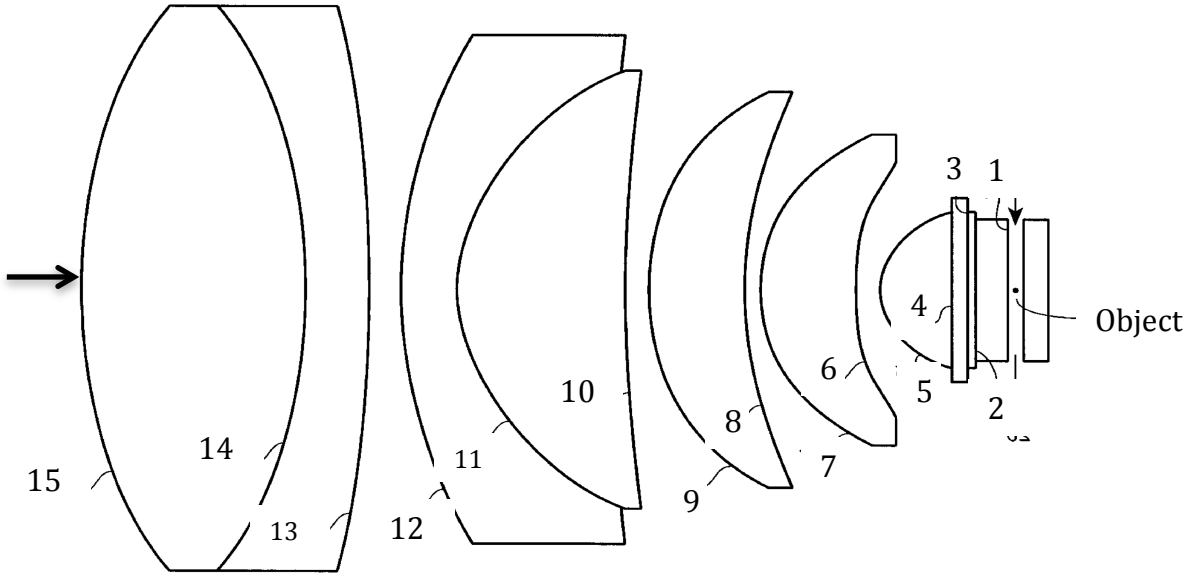

Figure 8 -Example of a generic objective lens (flow cytometry lens system) displaying the comprising lens elements with refractive surfaces that are displayed in Table 8 in Appendix 1. The elements within this lens were optimised to provide a working distance of at least 1.75mm, and a lens magnification greater than 10.

This generic lens shown in Figure 8 was provided with all the information necessary to calculate the increase in pulse duration (Appendix 1). This information included the material name and the thickness of each element. The corresponding Sellmeier co-efficient for each individual element was found [12] and the increase in pulse duration was calculated using Equations (28). The final output pulse duration after on-axis propagation for a 100 fs pulse at a wavelength of 800 nm was found (Appendix 2). According to Equation (7) discussed earlier, the output pulse duration is dependent upon the initial pulse duration and wavelength of the incident light and therefore the same calculation using Equation (28) was carried out over a range of initial pulse durations (τ_o=1-500 fs) and wavelengths (λ= 700-960 nm) to determine how the output pulse duration varies. The results are shown in Table 1.

2.3.2 Pulse duration through a generic 20x/0.75 NA objective lens

In order to determine the pulse duration off-axis, the length of glass through which the pulse propagates must also be known. As the laser pulse propagates through an objective lens, the outer part of the beam will follow a different path from that of the centre in accordance with Snells law [10]. After further research, an objective lens, which displays a higher degree of similarity to that which has been studied to provide the greatest imaging depths in TPLSM [8] was found i.e. with a low magnification and a high numerical aperture (NA)(20X Nikon 0.75NA). The data provided included the thickness of glass, radius of curvature and the Abbe number. This data was entered into the objective lens design software called Code V [46], (Synopsys, Optical Research Associated)), to produce the objective lens displayed in Figure 9. The software was set to display 7 rays entering the objective lens at different locations on the back aperture of the lens and displays the path they take through it at equal distances apart (approx. 1mm), one of which was on axis and three on either side. Below displays the diagram produced by Code V, which shows each individual element within the objective lens.

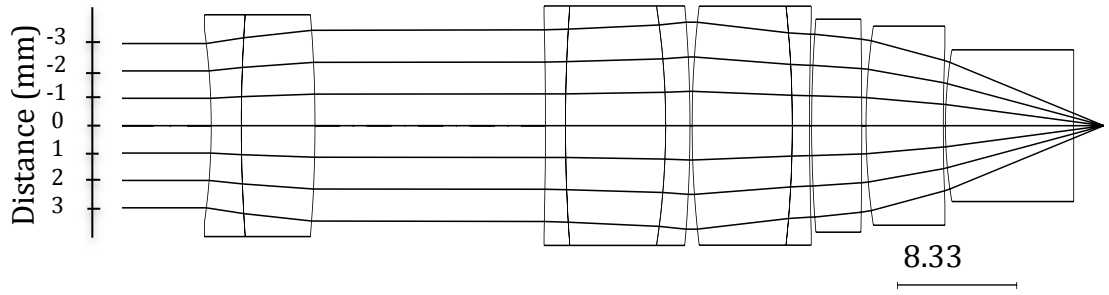

Figure 9 – Diagram of a generic 20 X Nikon lens with a NA of 0.75 was composed using lens design software Code V, where the ray starting at -3, -2, -1 are 3, 2 and 1 mm off axis to the left, 0 is on-axis and 1, 2 and 3 mm are 1, 2 and 3 mm off-axis to the right respectively.

Figure 9 was then opened in the freely available ImageJ (NIH) software, which can be easily attained from the Internet, in order to calibrate each pixel to a known thickness of material. This thickness was attained by first measuring the thickness that corresponds to one pixel. This was carried out by measuring the number of pixels within the 8.33 mm scale provided by Code V, which is shown on the bottom right hand corner of Figure 9. Then calculating the distance that corresponds to one pixel by dividing 8.33 mm by the number of pixels measured. ImageJ provides a calibration option, which allowed the calibration of one pixel to a known distance and in doing so, allowed the measurement of any distance on the objective lens giving the distance in mm as opposed to in pixels. The thickness of each individual element through which all 7 rays propagated was measured as mentioned and the results are displayed in Table 11 in Appendix 3. In order to confirm that the distances obtained using ImageJ were valid, the values on axis (at point 0 shown in Figure 9) were compared to the thickness of glass provided with the lens data, which should provide similar, if not identical, values if a correct calibration has been implemented.

Important information that was not provided was the material of each element and therefore we had to find the element material by comparing the Abbe number provided with the lens data to the Schott Catalogue [12]. The exact material could not be found and therefore estimations had to be made by ensuring that the material chosen had as close to the actual Abbe number and refractive index as possible. Once sensible estimations had been made, the increase in pulse duration for each ray was then calculated in the same way as previous for the cytometry lens (using Equation (28)) only this time taking the off-axis pulse durations into account. The variation in off-axis measurements is shown in Figure (10) for the increase in pulse duration after propagating through a single objective lens and in Figure (11) for a pair of objective lenses. The measurements obtained for propagation through a pair of lenses was carried out in order to compare with results which will be further discussed in Chapter 2.

The on-axis output pulse durations were taken for the Nikon lens over the same wavelength and initial pulse duration range as previously used for the cytometry lens, with the values shown in Table 2.

2.3.3 Probability of two-photon absorption

The probability of TPA to occur after propagation through both generic lenses (10x/1.2NA and 20x/0.75 NA) was then calculated using Equation (10). For the 20x Nikon lens, a typical value of the average power for TPLSM of 30 mW [47] was used, NA=0.75, and the repetition rate of a Ti:Sapphire laser is typically 76MHz. These values were kept constant throughout the calculation whereas the other values such as the two-photon cross-section of the fluorophore, wavelength and pulse duration were all varied. However, when calculating the TPA for the cytometry lens the higher NA associated with this lens allowed the average power to be reduced to 10 mW otherwise saturation would occur. This is because according to Equation (10) the probability of TPA is proportional to $(NA)^4$ and since the cytometry lens has a higher numerical aperture of 1.2 the average power must be reduced to compensate for the saturation that would be observed at 30 mW. The output pulse durations shown in Table 1 and 2 at each wavelength were used to calculate the probability of TPA for a common fluorphore used in microscopy, fluorescein [12] (Appendix 4). The two-photon cross sections are wavelength dependent and these values for fluorescein were obtained from a study carried out by M. A. Albota et al [24], which had a concentration of 14.5 μM in H_20. The results are shown in Figure 12 and 13 for the probability of TPA over the same wavelength and input pulse duration shown in Table 1 and 2 respectively to determine which input parameters would provide the highest probability of TPA.

2.4 Results

2.4.1 Cytometry lens (on-axis)

Initially the on axis results were calculated using a duration of a 100 fs pulse at a wavelength of 800 nm propagating through a generic objective lens used in flow cytometry (Figure 8). The generic lens used was also provided with the lens material and thickness [48], which was needed in order to carry out the necessary calculations. In doing so the pulse duration was calculated to have increased to 121 fs from 100 fs after one objective lens. The effect of different combinations of initial pulse durations and wavelengths on the output pulse durations is shown in Table 1.

Wavelength (nm)	1 fs	10 fs	50 fs	100 fs	140 fs	200 fs	500 fs
700	8500	850	178	131	152	204	500
720	8200	820	171	129	152	204	500
740	7800	780	164	127	151	204	500
760	7500	750	158	125	150	203	500
780	7200	720	153	123	149	203	500
800	6900	690	147	121	148	203	500
820	6600	660	142	120	148	203	500
840	6400	640	137	119	147	203	500
860	6100	620	132	117	147	202	500
880	5900	590	127	116	146	202	500
900	5600	560	123	115	146	202	500
920	5400	540	119	114	145	202	500
940	5100	510	114	112	145	202	500
960	4900	490	110	111	144	202	500

Table 1 – The output pulse duration through a cytometry lens (10x/1.2 NA) [7] with different combinations of wavelength and initial pulse duration. The highlighted results (in red) show the suggested operating conditions, based on the two-photon absorption efficiency increasing at shorter pulse durations as per Equation (10).

As shown in Table 1 the output pulse duration is dependent upon the input pulse duration and wavelength and therefore choosing the correct input parameters is paramount in achieving the maximum probability of TPA. The columns highlighted between and including 50–200 fs indicates the preferred pulse durations for two-photon microscopy, where the combination of input pulse durations and

wavelengths produce the shortest output pulse durations and as such higher probability of TPA.

2.4.2 20x/0.75 NA Objective lens (on and off-axis)

Code V was used to create a ray trace of the rays propagating through a Nikon lens (20x/0.75NA), which is relevant to TPLSM as opposed to the cytometry lens used before. Figure 9 displays seven rays propagating through the objective lens, each of which is travelling through a different length of glass. This length was found using ImageJ and the values are shown in Appendix 4. When taking the errors into account, the on-axis distance of each element through which the pulse propagated (which was measured using ImageJ) was the same as the thickness of each element provided by Patents Online [8]. This ensures an accurate calibration has been made and can therefore rely on the distances of each element for off-axis measurements.

A calculation was carried out by taking the dispersion due to the air between each element into account, however no difference to the pulse duration was calculated and was therefore considered negligible throughout the entire calculation. Using the thicknesses measured in Table 11, the increase in pulse duration for a 100 fs pulse at a wavelength of 800 nm was found to increase to approximately 125 fs on axis when using Equation (28) and the pulse duration varies as shown in Figure 10 as the input beam scans across the back aperture of the objective lens.

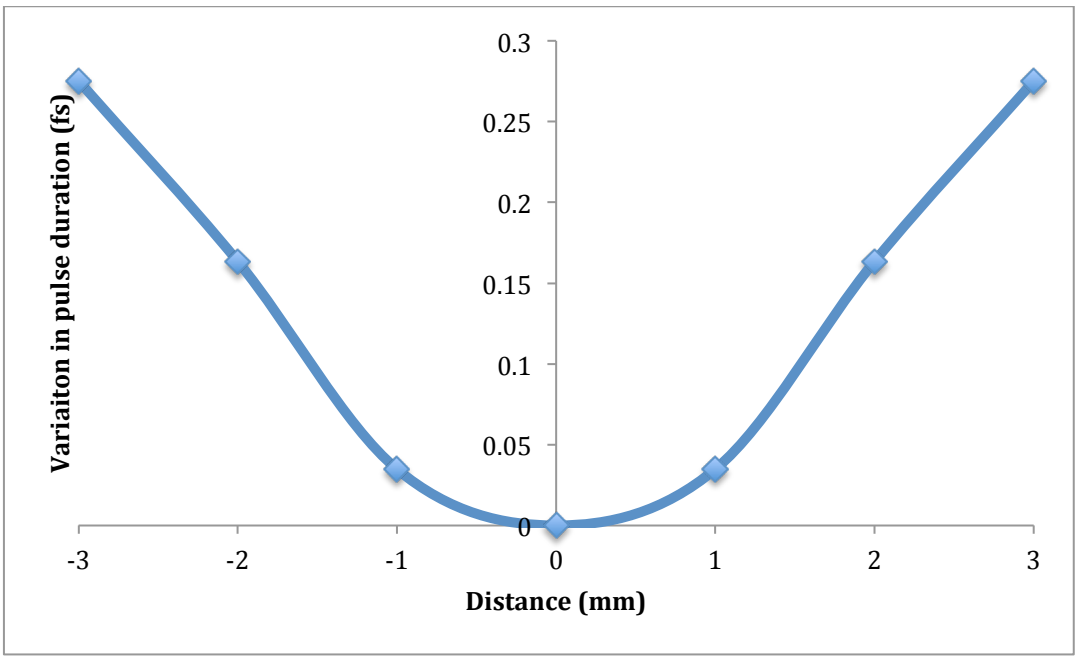

Figure 10 - The change in pulse duration going off axis for each ray shown in Figure 9 through one 20x/0.75NA objective lens [8].

As shown in Figure 10, the numerical model suggests that sub-fs changes in pulse duration are calculated as the laser beam propagates through different points of the objective lens' back aperture. Figure 11 shows how the output pulse duration varies for all seven rays after propagating through a pair of objective lenses to compare with measurements, which were made experimentally as explained in the next chapter.

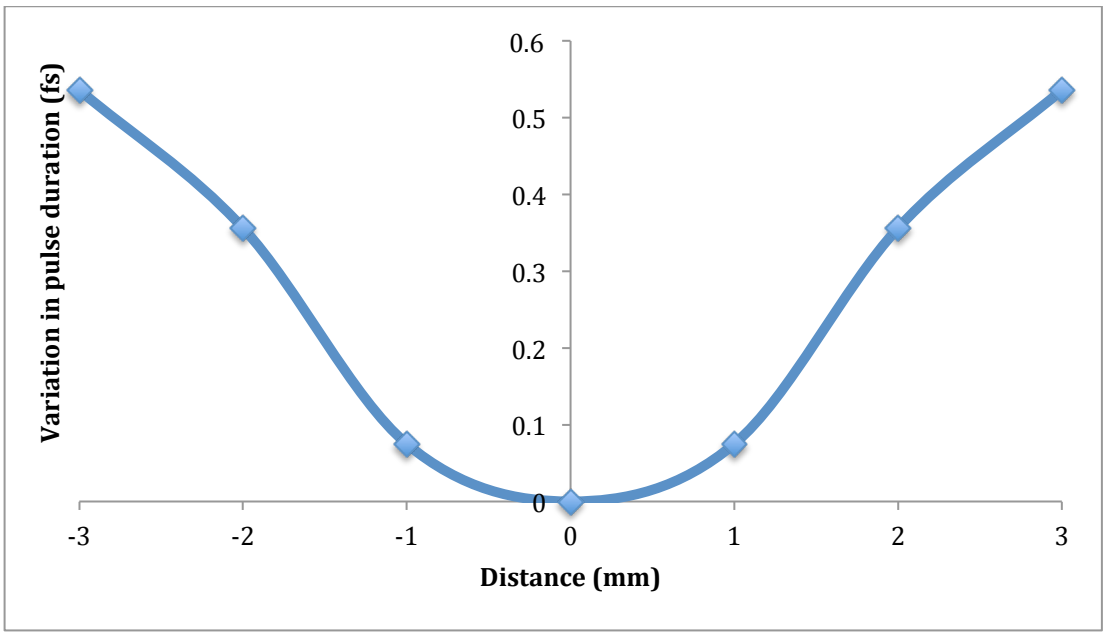

Figure 11 -The output pulse duration for each ray shown in Figure 9 through a pair of 20x/0.75 NA objective lenses [8].

On-axis the pulse duration had increased to 181 fs from 100 fs and again with sub-fs changes off-axis, which can be considered negligible since no optoelectronic measuring technique can measure such precision, because most commercial autocorrelators can only measure as accurate as a few fs [49].

Following Equation (33-35), it can be calculated that Equation (34), for the 20x/0.75 NA objective lens, has a solution of 1.14. When inserting this value into Equation (35) it gives an output pulse duration of 125 fs after one objective lens, which agrees with the pulse duration calculated previously. We now have a suitable method (Equation 33-35) to determine the pulse duration after any objective lens so long as we have a known input and output pulse duration after propagation through a pair of identical objective lenses.

The data so far has been calculated with an initial pulse duration of 100 fs at a wavelength of 800 nm, so by changing these variables we can determine what effect this has on the output pulse duration as shown in Table 2 below.

Wavelength (nm)	1 fs	10 fs	50 fs	100 fs	140 fs	200 fs	500 fs
700	9200	920	191	136	155	205	500
720	8800	880	184	133	154	205	500
740	8500	850	177	131	153	204	500
760	8100	810	170	129	152	204	500
780	7800	780	164	127	151	204	500
800	7500	750	158	125	150	204	500
820	7200	720	153	123	149	203	500
840	6900	690	147	122	148	203	500
860	6700	670	142	120	148	203	500
880	6400	640	137	119	147	203	500
900	6100	610	133	117	147	202	500
920	5900	590	128	116	146	202	500
940	5600	560	123	115	146	202	500
960	5400	540	119	114	145	202	500

Table 2 - The output pulse duration through a Nikon objective lens (20x 0.75NA [8]) with different combinations of wavelength and initial pulse duration. The highlighted results (in red) show the suggested operating conditions, based on the two-photon absorption efficiency increasing at shorter pulse durations as per Equation (10).

Again, the columns highlighted between and including 50-200 fs indicates the preferred pulse durations for two-photon microscopy, where the combination of input pulse durations and wavelengths produce the shortest output pulse durations and as such higher probability of TPA. The data also shows that above 200 fs there is no measureable effect (below sub-fs) in pulse duration as shown in the 500 fs column for both the cytometry and the Nikon lens.

2.4.3 Probability of two-photon absorption

The probability of TPA occurring using both generic lenses was calculated for fluorescein with a concentration of 14.5 µM in H_20. This was achieved by using Equation (10) of Chapter 1, along with the two-photon cross section of fluorescein [48] at each wavelength and the output pulse durations shown in Table 1. All other parameters were kept constant i.e. for the cytometry lens P_{ave}=10 mW, NA=1.2 and Δν=76 MHz. Figure 12 below displays this probability over the same wavelength and input pulse duration range.

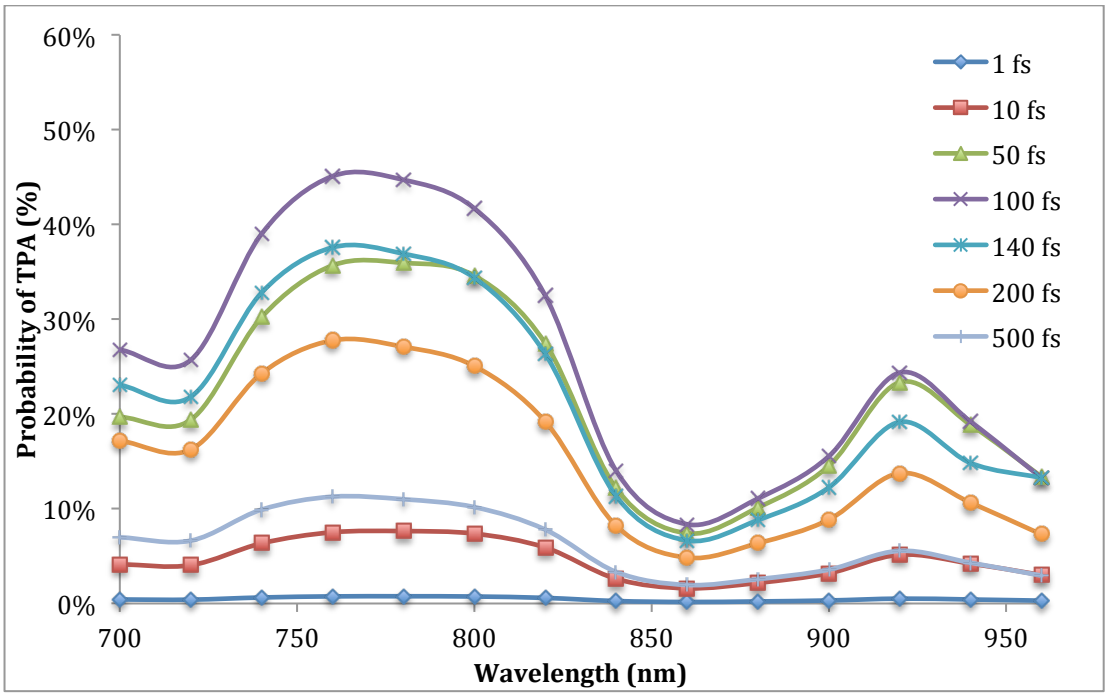

Figure 12 - The probability of TPA through a Nikon lens using the output pulse durations from Table 1 with an average power of 10 mW.

The input parameters used for the Nikon objective lens were the output pulse durations used in Table 2, P_{ave}=30 mW, NA=0.75 and Δν=76 MHz. Figure 13 below displays this probability over the same wavelength and input pulse duration range.

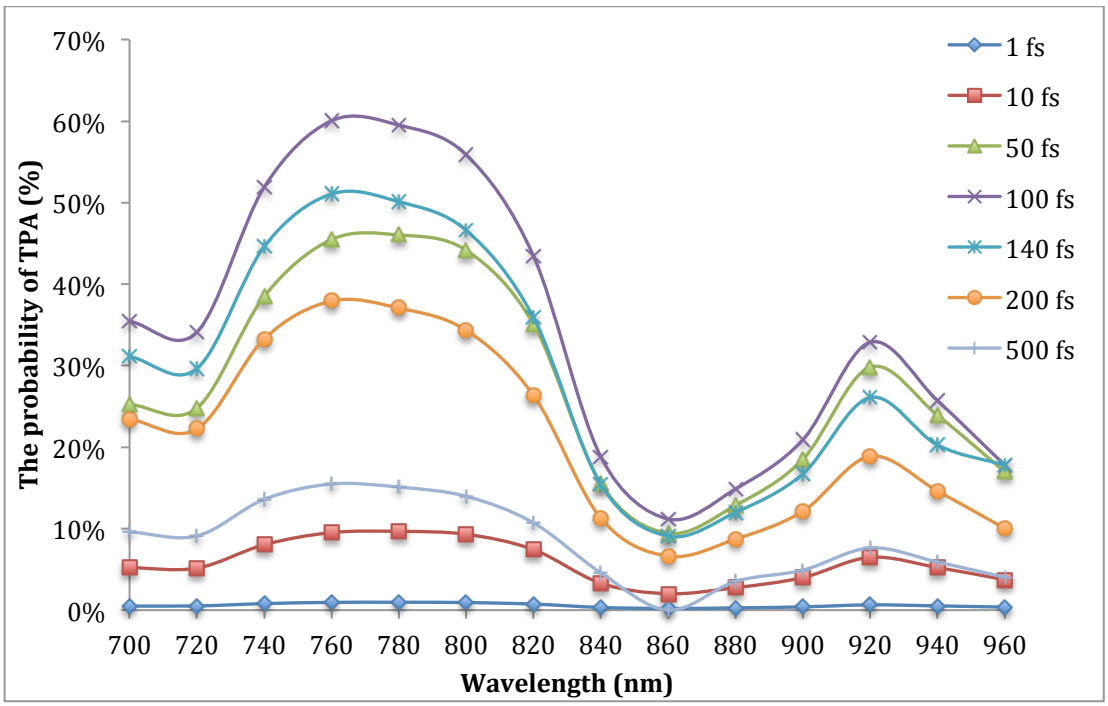

Figure 13 - The probability of TPA through a Nikon lens using the output pulse durations from Table 2 with an average power of 30 mW.

From these data it can be established that the optimum wavelength and initial pulse duration to use for both lenses using this particular fluorophore is 100 fs at a wavelength between 740-800 nm, which produces the highest probability of TPA. The dip seen between 840-900 nm corresponds to a decrease in value for the two-photon cross sections of fluorescein between these particular wavelengths, which will obviously vary between fluorophores depending on the two-photon cross section values (some of which are provided in [50]).

2.5 Discussion of results

By demonstrating the dependence of TPA upon the pulse duration and wavelength we have emphasized the importance of obtaining as short a pulse duration as possible at the sample plane. Table 1 and 2 shows that material dispersion has an increased effect on the shorter pulses, since the shortest possible pulses that are required for microscopy such as a 10 fs pulse at a wavelength of 800 nm has the potential to stretch to a higher value than a 500 fs pulse at the same wavelength.

To analyse the extent to which the pulse duration varies as the laser beam scans across the back aperture of an objective during microscopy the on and off-axis output pulse durations were calculated for a generic 20x/0.75 NA Nikon objective lens typically used in TPLSM. A 100 fs pulse at a wavelength of 800 nm was calculated to increase to 125 fs and the change in pulse duration off-axis was sub-fs as shown in Figure 10. Therefore the effect of material dispersion on the pulse duration can be considered constant across the lens. In the next chapter, the temporal dispersion through two objective lenses will be measured experimentally and was therefore calculated to compare magnitudes. On-axis the pulse duration was calculated to be 181 fs with similar sub-fs changes for off-axis values. By comparing the 25 fs increase through the first objective lens to the 56 fs increase through the second objective lens (181 fs subtract 125 fs) we can see that this agrees with Figure 7, which shows that it takes some level of propagation for the pulse frequencies to completely separate before the pulse duration increases linearly.

The output pulse duration was also calculated for a combination of different wavelengths and input pulse durations to determine a suitable area that would be best to work with in TPLSM. The shortest pulse durations were calculated between 50-200 fs at any wavelength for both lenses shown in Table 1 and 2. Using all the output pulse durations displayed in Table 1 and 2, the corresponding probability of TPA to occur was calculated using Equation (10) for Fluorescein. From the graph

produced (Figure 12 and 13) it could be shown that there was a clear wavelength and initial pulse duration range at which the highest probability would occur. This range was between 50-200 fs between a wavelength range of 740-820 nm. Other points can also be noted from this graph, one of which is the cross over in the probability at certain points such as between 50 fs and 140 fs at a wavelength of 960 nm. This can be useful for certain studies that prefer to work with higher wavelengths. The plot also shows that at several points there is little or no difference between the pulse with an initial duration of 50 fs or 140 fs between a wavelength range of 820 - 880 nm.

2.6 Conclusion

This chapter has demonstrated a reliable simulation to calculate the output pulse duration after propagating through different points of an objective lens. This is an important measure in microscopy since in TPLSM the laser scans across the back aperture of the objective lens [50] and as a result temporally dispersing ultrashort pulses (Equation(26)) [24]. Any change in pulse duration as the laser scans across the lens has a direct effect on the probability of TPA (Equation (7)) and therefore decreasing the resolution of the microscopic images. The objective lenses used to illustrate this numerical simulation [11] did not display a significant change in output pulse duration across the back of the lens, with less than 1 fs change through the 20x Nikon objective lens. However, a 100 fs pulse at a wavelength of 800 nm was calculated to increase by 25 fs for the Nikon lens and 21 fs for the cytometry lens. As shown in Figure 13, the shortest pulses required for TPLSM (such as 10 fs pulse) has a less than 10% probability of TPA and therefore the objective lenses discussed may benefit from employing a dispersion compensation technique. The cytometry and Nikon lens used were manufactured several years ago (2003 and 2001 respectively) and therefore may not contain the exact same internal elements within the objective lens. The next chapter will produce experimental data of the on and off-axis pulse durations through objective lenses commonly used in microscopy.

Chapter 3 - Experimental measurement of pulse broadening in commercial microscope objective lenses: on-axis and off-axis

3.1 Introduction

It is possible to calculate the output pulse duration after propagation through an objective lens when the internal elements are known using the previously shown method in chapter 2. However, these data are almost never available because large companies have confidentiality agreements on most of their products to discourage competitors from enhancing them. Therefore to calculate the pulse duration after one objective lens of unknown material, another step has to be introduced by measuring the pulse duration through a pair of objective lenses using an autocorrelator and calculating the pulse duration after one objective lens. This chapter will demonstrate an experimental method of obtaining the pulse duration after propagation through any objective lens on and off-axis using two Nikon objective lenses (10x/0.45 NA and 20x/0.75 NA) and the theory shown in Chapter 2.

3.2 Theory

3.2.1 Lasers

Laser microscopy relies on focusing by use of a series of lenses. The simplified purpose of these lenses with almost perfect axial symmetry is to transmit and focus light. Much of optics is based on common processes that fall in the category of linear optics such as reflection, refraction, diffraction, superposition etc. However there is another category known as non-linear optics, which arises at very high light intensities. Non-linear optics is used when the irradiance of light becomes too high to abide by the principle of superposition, which can be applied in linear optics. The laser (Light Amplification by Stimulated Emission of Radiation) has been said to be "perhaps one of the most important optical devices in the past 50 years" [51], which

changes electrical (or optical) energy into intense, highly directional, nearly monochromatic, electromagnetic wave energy.

3.2.1.1 Ti:Sapphire (Ti:Al_2O_3) laser

As discussed the Ti:Sapphire laser is a preferred choice for TPLSM based on its ability to wavelength tune and generate ultrashort pulses which was required to analyse the effect of material dispersion upon the pulse duration. It has the ability to operate in both cw as well as mode-locked (ML). The latter term refers to the fact that the laser is locking different frequencies together to produce a train of pulses. This usually occurs with a repetition rate of approximately 76MHz. As its name 'Ti:Sapphire' suggests, the lasing medium within the laser is a crystal sapphire doped with titanium ions, which is often optically pumped by a second laser of wavelength 514-532 nm. In this study, it was a frequency doubled Nd:YVO_4 crystal laser used to pump the Ti:Sapphire gain material. This technique of optical pumping uses light energy to excite the atomic electrons from a ground state to an excited state, as previously discussed, until a population inversion is reached.

3.2.1.2 Theory of Mode-locking

Mode-locking is the term which is more widely recognised as a method of producing ultrashort pulses within a laser cavity [11]. Laser pulses as short as a few femtoseconds (10^{-15}s) have been obtained. These ultrashort pulses have a much higher peak power than the output power of a cw laser.

The concept of mode-locking involves collectively locking several longitudinal modes together so that oscillation by the laser occurs on all of them simultaneously. The number of modes that are in phase with each other determines the duration of each pulse emitted by the laser system. The relation between the pulse duration and the number of modes is given by [52]:

$$\Delta\tau = \frac{0.32}{N\Delta\nu} \quad \text{....(36)}$$

where Δτ is the pulse duration, N is the number of modes, Δν is the frequency separation and 0.32 is the value for the time-bandwidth product of ultrashort pulsed lasers, which produce hyperbolic secant pulse shapes ($sech^2$). NΔν is known as the mode-locked bandwidth and since 0.32 is a fixed value the larger the mode-locked bandwidth the shorter the pulse duration.

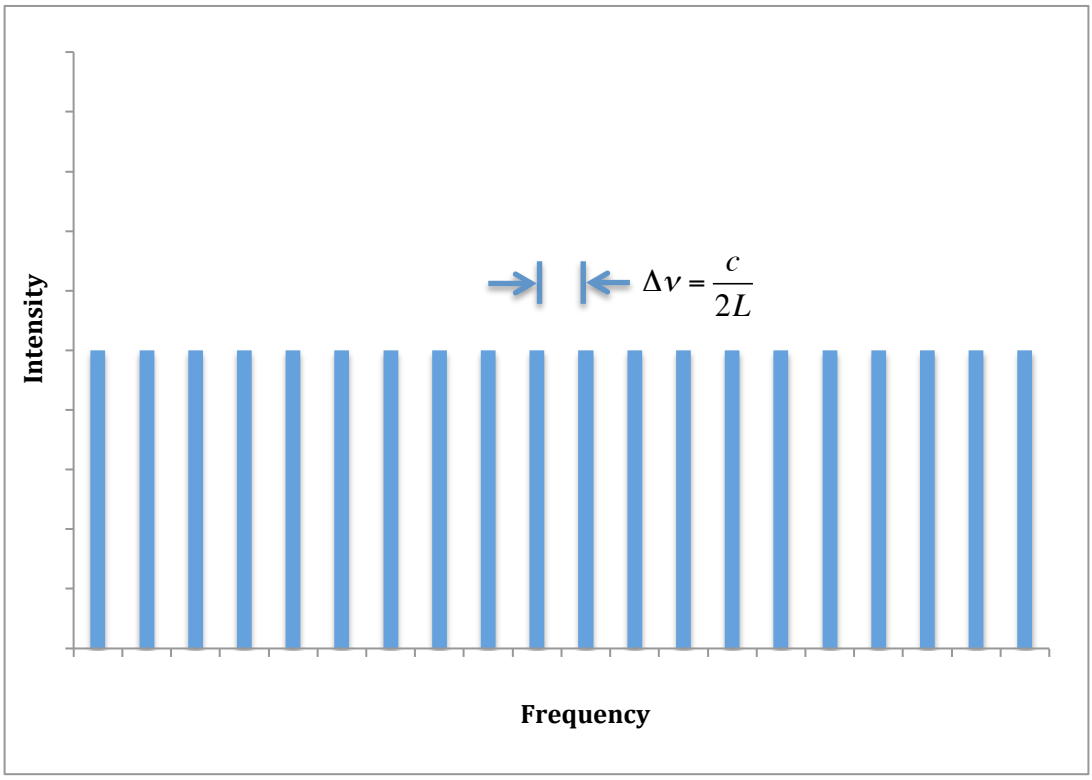

Figure 14– Illustration of the cavity longitudinal mode structure, with each mode separated by the repetition rate equal to the speed of light divided by two times the laser cavity length.

The following equations are able to describe the total optical electric field resulting from multimode oscillation [52]:

$$U(t) = \sum_{-(N-1)/2}^{(N-1)/2} e^{i(\omega_0 + n\omega)t} \quad \text{...(37)}$$

which can also be written in a simpler form:

$$U(t) = e^{i\omega_0 t}\frac{\sin(N\omega t/2)}{\sin(\omega t/2)} \quad ...(38)$$

where ω is the oscillation frequency.

The laser output power averaged over one optical cycle is proportional to:

$$P(t) \propto \frac{\sin^2(N\omega t/2)}{\sin^2(\omega t/2)} \quad ...(39)$$

This expression shows that the peak power increases with the number of modes present within the cavity. This can also be shown by the following plot of the power as a function of time for N=5, 11 and 15.

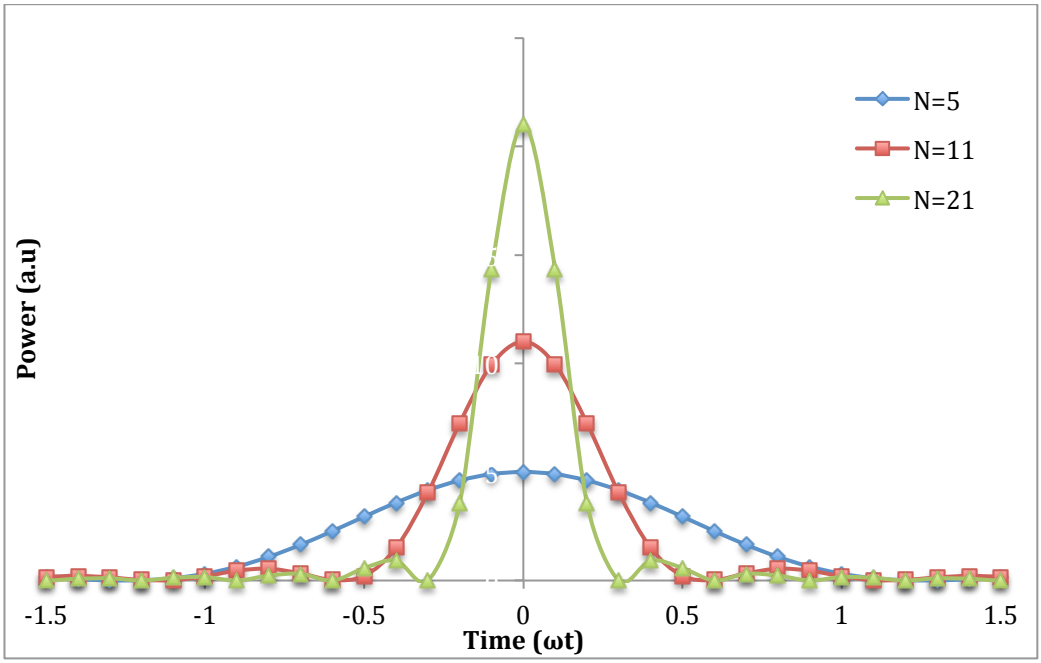

Figure 15 - Average power as a function of time for different values of N using Equation (39).

Figure 15 also illustrates the effect the number of modes has on the pulse duration as described in Equation (36), where a higher increase in the number of modes

produces the shortest pulse durations. This can be seen by the difference in the FWHM between N=5 and N=21.

The Ti:Sapphire laser is based on Kerr lens mode-locking, which is a passive mode locking technique that uses an artificial saturable absorber system [53]. This process of mode-locking controls a group of photons, which are continuously travelling between the laser mirrors at either end of the cavity. As the photons arrive at the Kerr lens mode-locker situated within the cavity the locker opens to allow the photons to transmit through. In this case, a mechanism such as a self-adjusting modulator is introduced to open the shutter in order to allow the passing of photons as they approach the shutter but is otherwise closed and therefore does not rely on the shutter being open when approaching it (active mode-locking).

Saturable absorption is often implicated into the design of lasers acting as a self-adjusting modulator, which relies on the basis of pulses having a higher intensity than that of cw. In the presence of increasingly high intensity pulses the beam size decreases as a result of self-focusing, which is produced by the non-linear refractive index change of the medium or rod [54], [55]. In turn this reduces the refraction of light as it passes through a refracting element. A greater thickness of glass at the centre of a lens compared to its edges is a good illustration, which subsequently causes the centre of the beam to slow down more than the edges and as a result causes the light to bend towards the centre. Another way of forming a lens like system is by changing the refractive index of a medium to be higher in the centre, gradient index lens. The optical Kerr-Lens system employs this theory, since at appropriately high light intensities the atoms of the material become distorted consequently changing the refractive index [36]. Since the intensity within the centre of a laser beam has a much higher intensity compared to its edges, the refractive index changes across the profile of the beam causing a greater refractive index to form in the centre as opposed to the edges.

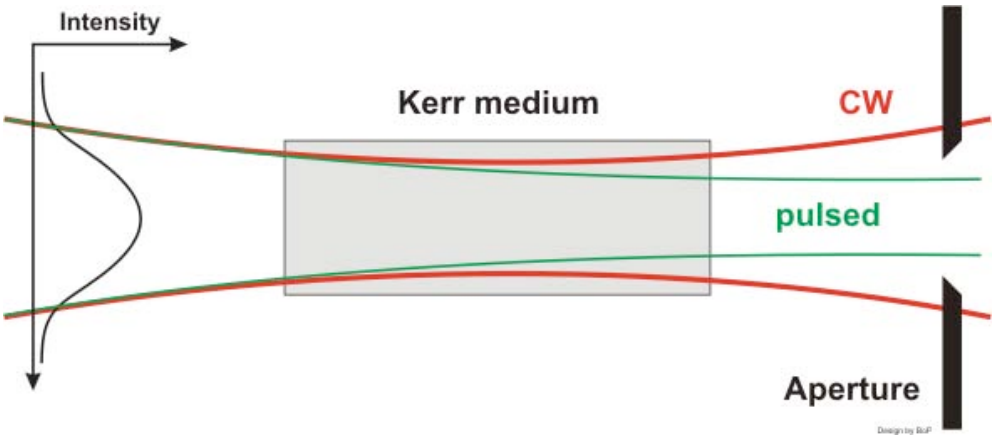

Figure 16 -Kerr lens mode-locking [56].

The depletion of larger beams, i.e. cw, can be achieved using a simple slit or aperture located at the laser output. As a result a device has therefore been created to narrow the beam width of the laser beam and with the addition of the slit mentioned earlier a saturable absorber system has been formed which creates a powerful technique for mode-locking (Figure 16).

3.2.2 Autocorrelator

Most commonly known methods of measuring optical characteristics such as photodiodes and oscilloscopes don't have the response time capable of measuring the sub-fs pulses produced by mode-locked lasers [57]. Autocorrelation is a widely used method in determining the width characteristics of a laser pulse on a fs timescale. Intensity autocorrelation is an example, which was one of the first techniques attempted in the 1960's based on measuring the intensity of a pulse as a function of time and therefore estimating the duration of an ultrashort pulse. This process of correlation occurs by splitting the pulse into two separate pulses of equal intensity using a beam splitter (Figure 17), causing one beam to lag behind the other.

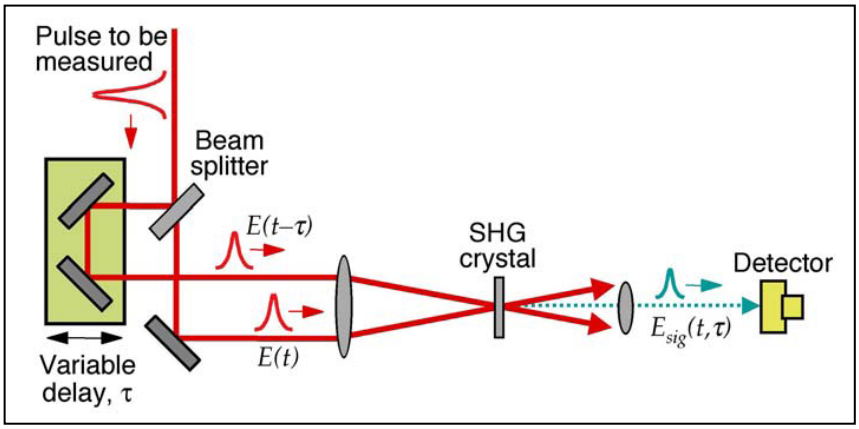

Figure 17 -Layout of intensity autocorrelator [58].

The two split beams are spatially overlapped onto a non-linear optical medium (second harmonic generating crystal) producing a signal, twice the frequency of the input light with a field envelope given by [58]:

$$E_{sig}^{SHG}(t,\tau) \propto E(t)E(t-\tau) \quad ...(40)$$

where τ is the delay from time t. This field envelope has an intensity, which is proportional to the multiple of the intensities of each input pulse given by:

$$I_{sig}^{SHG}(t,\tau) \propto I(t)I(t-\tau) \quad ...(41)$$

This beam cannot be easily resolved in time and therefore the detector will measure the intensity autocorrelation signal given by:

$$A^{(2)}(\tau) = \int_{-\infty}^{\infty} I(t)I(t-\tau)dt \quad ...(42)$$

where the superscript (2) shows that it is of second harmonic generation. This signal is detected, which then shows the temporal profile of the autocorrelation signal. Using the generated profile, the pulse duration can be determined by estimating the full-width at half maximum (FWHM), which is provided by the autocorrelator. For this

particular study, we are assuming a $sech^2$ pulse shape and therefore have a de-convolution factor of 1.54 to take into account. By multiplying the autocorrelation signal by the 1.54 de-convolution factor it provides us with a pulse duration for this particular pulse shape. This factor changes depending on the pulse shape i.e. for a Gaussian shaped pulse the factor becomes 1.414. Other analysis techniques have now been implemented such as frequency resolved optical gating (FROG), Grating-eliminated no-nonsense observation of ultrafast incident laser light e-fields (GRENOIULLE) and Spectral phase interferometry for direct electric field reconstruction (SPIDER), all of which provide the temporal profile of a pulse. However, these techniques are far superior in that they can also provide pulse phase information [59]. However, for the purpose of this study the autocorrelator provides all the necessary information needed to measure the material dispersions effect upon ultrashort pulses.

3.3 Experiment

3.3.1 Average Power

First, the average output power of the Ti:Sapphire laser (Coherent Mira 900-F) was measured in order to check its performance level. This was carried out by firstly ensuring the laser was mode-locked by adjusting the birefringent filter (BRF) whilst simultaneously adjusting the Brewster prism position to minimise GVD. Once mode-locked, the wavelength spectrum could be measured using a standard spectrum analyzer [model: E200; IST-REES], connected to an oscilloscope, where the situated peak of the spectrum determined the wavelength of the Ti:Sapphire laser. The average output power through a wavelength range of 725-885 nm was measured using a power meter [model: 407-A; Spectra Physics] every 10 nm. The results were plotted of average output power as a function of wavelength shown in Figure 20. This is a very useful technique in determining the efficiency of the laser and can establish any faults or degradation within the system as well as determining the most reliable wavelengths at which to work.

3.3.2 Set-up for measuring the pulse duration through a pair of objective lenses

Having studied the average output power over a range of wavelengths, the pulse duration was then analysed using an autocorrelator [model: APE, Pulse Check] [59], [60]. Again, the Ti:Sapphire laser was mode-locked at a chosen wavelength, the spectrometer was then removed from beam path and the beam then directed into the autocorrelator using mirrors, which were chosen to reflect near infrared (IR) light. The pulse duration provided by the autocorrelator was taken several times at each wavelength as a result of fluctuation and any errors were calculated as the standard deviation from the mean. As mentioned in Chapter 2, it is very much suspected that the Ti:Sapphire laser produces a $sech^2$ pulse shape. Therefore the value for the FWHM of the autocorrelation signal was multiplied by the de-convolution factor to provide a pulse duration reliable with a $sech^2$ pulse shape [49].

The next step was in measuring the effect of material dispersion upon the duration of an ultrashort pulse after propagating through an objective lens of unknown material. Again, as briefly discussed in Chapter 2 a pair of objective lenses had to be used to collimate the beam in order for the autocorrelator to detect a signal. Therefore, the experiment was set up as shown in Figure 18. The two identical objective lenses were been placed nose-to-nose, separated by double the focal length until a collimated beam seemed to have formed. A knife-edge technique was carried out to ensure this was the case by measuring the beam diameter at two different locations. If a collimated beam is produced the width at both locations should be similar.

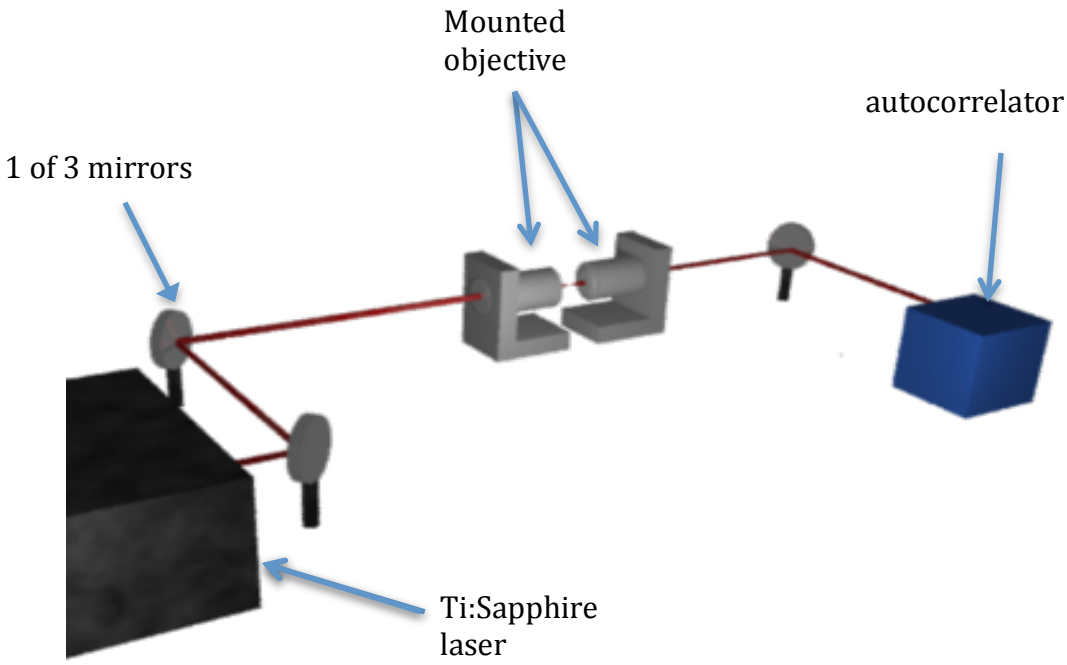

Figure 18 - Experimental set-up, showing the beam path from the Ti:Sapphire laser, through a pair of identical Nikon objective lenses and reflected into an APE autocorrelator by a series of near infrared (NIR) reflecting mirrors.

A pair of apertures were placed in the beam path before inserting the objective lenses in. The objective lenses were mounted on to a separate pair of translation stages, each with an x, y and z translation distance between 9-16 mm and placed in the centre of the beam path. The translation stages were altered slightly in each direction until the collimated beam passed through the centre of the two apertures. In doing so, it is assured that the laser beam is propagating directly on-axis through both objective lenses, producing a collimated beam, which has a pulse duration that can be measured using the autocorrelator. This is highly important since it ensures that an equal quantity of material dispersion through each objective lens will affect the pulse duration. The initial lens separation appeared to have formed a collimated beam, where the beam width at two different positions was calculated to be 0.7 mm and 0.8mm. Despite the beam widths not being identical it is acceptable to assume a collimated beam has been formed, which is adequate for autocorrelation.

3.3.3 Measuring the pulse duration through different pairs of objective lenses (10x/0.45 NA and 20x/0.75 NA)

A way of measuring the off-axis pulse duration after propagating through an objective lens is by obtaining the pulse duration at several different points of the back aperture of the lens (Figure 19). This should theoretically form symmetrical values for the pulse duration, as shown in Figure 10 and 11 of Chapter 2. Any increase in pulse duration would imply an increase in the thickness of the glass and vice versa. Having previously set up a reliable method of measuring the increase in pulse duration through a pair of objective lenses, the next step was to measure the increase in pulse duration using a pair of commercial objective lenses that are commonly used in laser microscopy (Nikon 10x/0.45 NA).

The Ti:Sapphire laser was mode-locked at a wavelength of 760 nm and the pulse duration was measured, without any lenses in the laser beam path, using the autocorrelator. Ten values were obtained and averaged to give an initial pulse duration of 130± 4 fs. The back aperture of the objective lenses both had a diameter of approximately 6mm and the pulse durations were obtained in increments of 1 mm (3mm up, down, left and right from the centre) as shown in Figure 19.

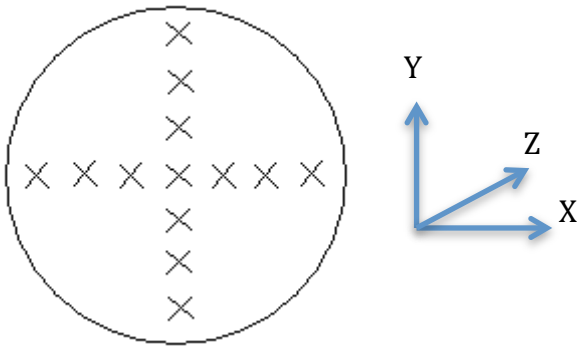

Figure 19- Schematic diagram displaying the points on the back aperture of the objective lens at which the laser beam started propagation.

The micrometer reading on each translation stage was altered by 1mm in the same direction, so that the incoming beam would propagate off-axis through an identical point of both objective lenses. The pulse duration was obtained 10 times after propagation through both lenses and averaged to obtain the increase in pulse duration through a pair of objective lenses. By referring back to Chapter 2 (Equations 33-35), the input and output pulse durations measured with the autocorrelator were then used to obtain the pulse duration after one single objective lens. The results obtained from the pulse durations across the x and y-direction are displayed in Figure 21 and 22 respectively.

Once the results had been analysed using the 10x/0.45 NA objective lenses the same experiment was carried out for two identical 20x/0.75 NA Nikon objective lenses in order to determine what effect a different lens pair would have upon the pulse duration. The pulse duration before propagation through the pair of objective lenses was measured to be 146 ± 5 fs and the final duration after propagation through one objective lens using the same method as the 10x objective lenses is displayed in Figure 23 and 24 respectively.

3.4 Results

3.4.1 Average power

Plotting the average output power as a function of wavelength produced the results as shown in Figure 20 below. From these results it can be determined that the optimum wavelength at which the Ti:Sapphire laser emitted the highest average power was approximately in the wavelength range of 825-860 nm.

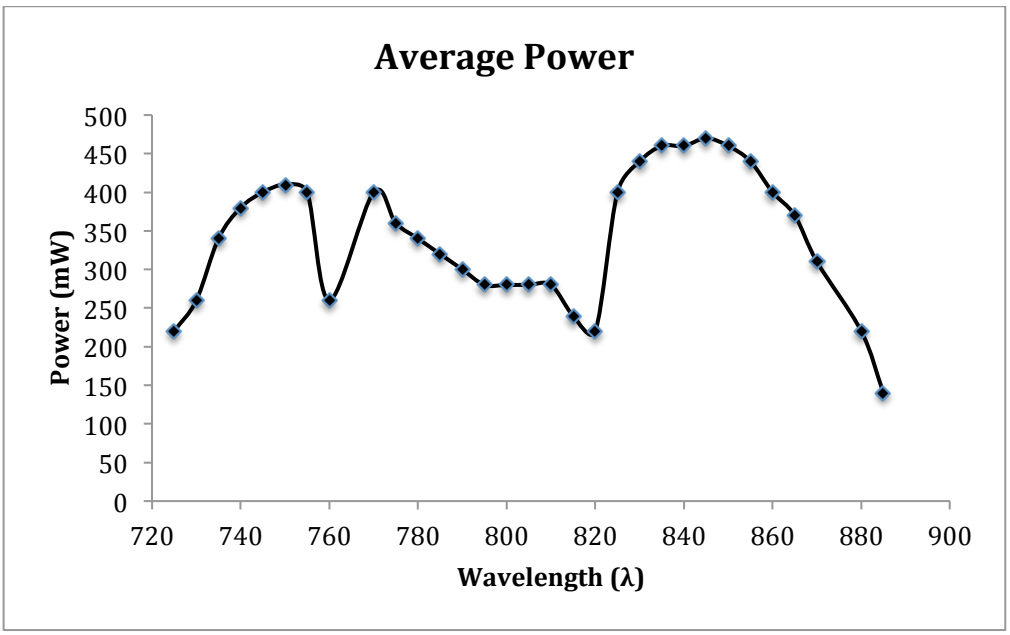

Figure 20 – Power output at specific wavelengths using a standard power metre [model: 407-A; spectra physics].

By referring to the previously mentioned Equation (9), which is a calculated parameter, obtaining the highest possible average power along with the smallest pulse duration directly increases the peak power that is required for most non-linear imaging such as two-photon microscopy, SHG etc. [61]. A high average output power is important since it allows shorter imaging time, deeper imaging depths and faster frame rates for quality imaging. Figure 20 therefore demonstrates that the wavelengths at which the highest average powers occurs are 750 nm, 770 nm and between 825-870 nm. The unusual trend between wavelengths 760-820 nm could be explained by misalignment within the laser, or water absorption.

3.4.2 Measuring the pulse duration through a 10x/0.45 NA objective lens

The pulse durations were obtained at different locations across the back aperture of the lens in the x and the y-direction of two 10x objective lenses in increments of 1mm with the results displayed in Figures 21 and 22 respectively.

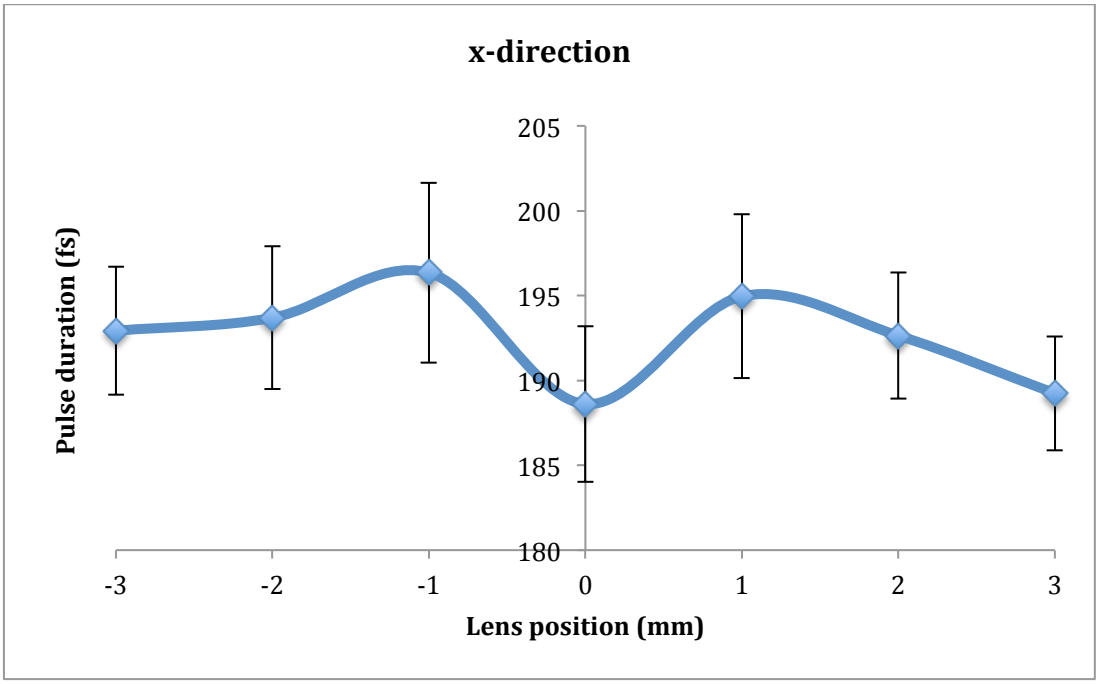

Figure 21 - The average pulse duration obtained across the x-direction of a 10x/0.45 NA Nikon objective lens, with an initial pulse duration of 130± 4 fs at a wavelength of 760 nm.

As can be shown from Figure 21 the results suggest that the thickness of glass appears to be symmetrical about the on-axis measurement, where the centre appears to have the least thickness of material since it displays the shortest pulse duration. The errors associated with each point have been calculated as the standard deviation of 10 values obtained at each position. Taking the error into account, the pulse duration across the back aperture of this particular pair of objective lenses appears to be constant since most of the averaged values fall between the error range of the other points.

When analysing the pulse duration in the y-direction an equal number of measurements on either side of the centre could not be obtained as a result of either the shape of the beam being astigmatic or the back aperture of the lens not being perfectly centred around the lens. As a result only measurements to 2mm down could be obtained for the pulse duration. None-the-less it provides us with data, which can be used to analyse the temporal dispersion across the lens.

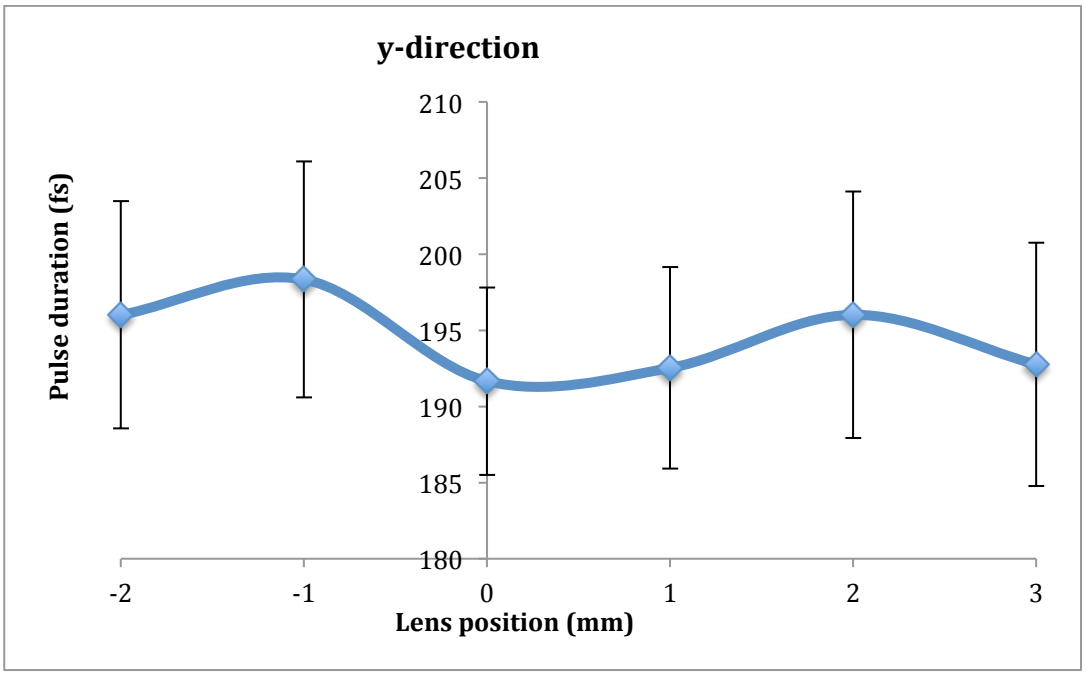

Figure 22 - The average pulse duration obtained across the y-direction of a 10x/0.45 NA Nikon objective lens. The initial pulse duration was measured to be 130 ± 4fs at a wavelength of 760 nm.

Measurements from -3mm could not be obtained for this particular objective lens because the outer casing surrounding the lens was perhaps centred off axis, which obstructed the light from propagating through the lens. However, a similar result is shown in Figure 22 compared to the data displayed in Figure 21, where the pulse duration appears to be symmetrical across the y-direction of the lens. However, in this case there is quite clearly a constant effect of material dispersion upon the ultrashort pulse across the y-direction of the objective lens since each point falls between the same error ranges.

3.4.3. Measuring the pulse duration through a 20x/0.75 NA objective lens

Below are the results obtained when measuring the pulse duration across the x and y-direction of an objective lens in increments of 1mm (shown in Figure 23 and 24 respectively), using a pair of 20x/0.75 NA Nikon objective lenses.

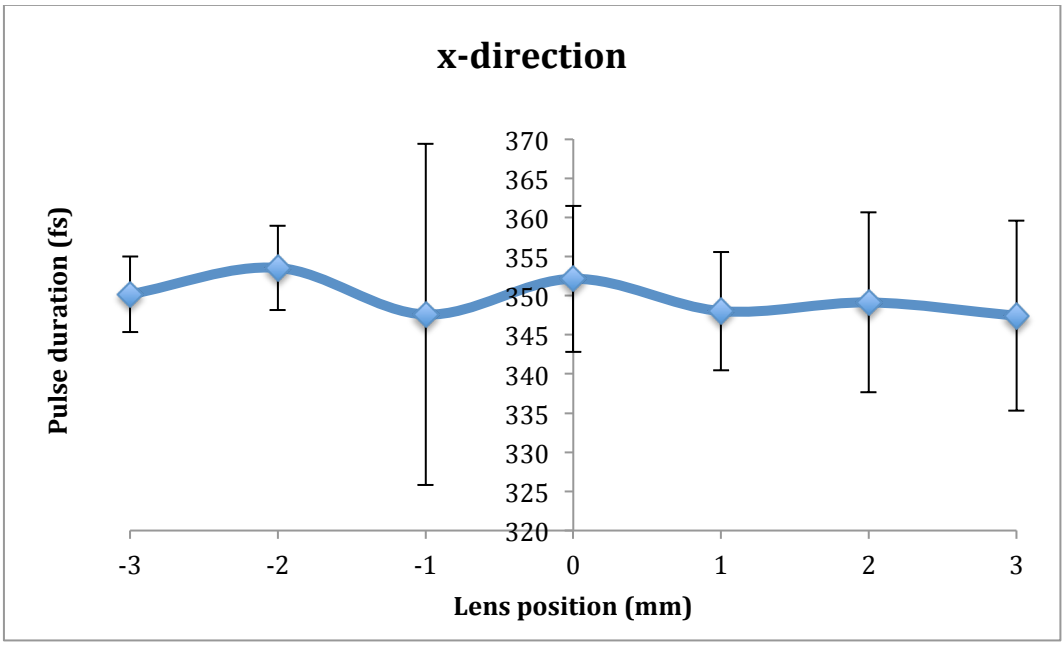

Figure 23 - Pulse durations obtained across the x-direction of a 20x/0.75 NA Nikon objective lens. The initial pulse duration was measured to be 146± 5 fs at a wavelength of 760 nm.

The results obtained in the x-direction appear to have a similar change in off-axis pulse durations compared to the results obtained with the 10x lenses (Figure 21) i.e. the change in the off-axis pulse durations appears to be within a 10 fs range for both. However, when comparing the pulse durations, lens position 1, 2 and 3 mm all appear to have the same pulse duration, which suggests no significant increase in pulse duration can be measured.

Finally, for completion the measurements were obtained for the pulse duration in the y-direction, which are shown in Figure 24 below.

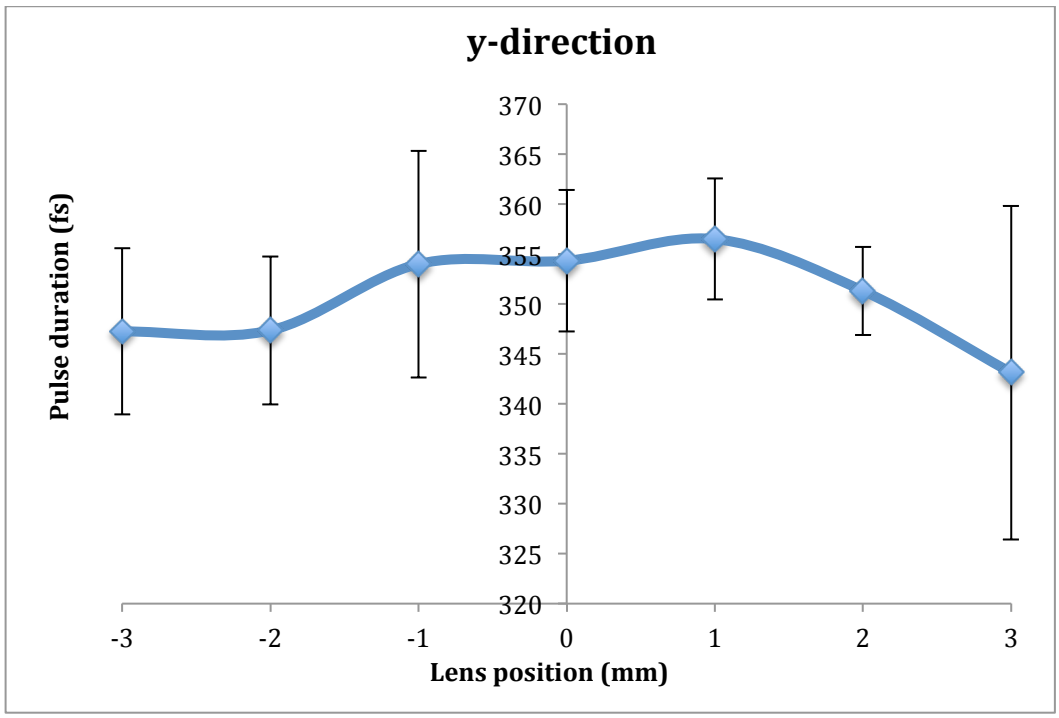

Figure 24 - The pulse durations obtained across the y-direction of a 20x/0.75 NA Nikon objective lens. The initial pulse duration was measured to be 146 ± 5 fs at a wavelength of 760 nm.

By comparing the x and y-direction measurements the two show almost opposite symmetry in the off-axis pulse durations, which again shows that no notable increase in pulse duration can be measured.

3.5 Discussion of results

The laser beam was propagated through a pair of 10x/0.45 NA and 20x/0.75 NA Nikon objective lenses on and off-axis in the x and y direction to display the extent of the problem during TPLSM. The measured output pulse durations after a pair of objective lenses were then used to calculate the pulse duration after one objective lens using Equation (33-35) of Chapter 2 and Figures 21-24 display these results. Despite all four figures showing almost symmetrical results off-axis from one side to the other, they do not follow the same trend as each other. Realistically the thickness of glass should be identical when measuring anywhere on the same radius from the centre of any one objective lens, which might have shown through if the scale of the problem was larger. As it is, the data does not show any clear trends when scanning across the objective lens. A possible explanation for this could rely on the fact that the autocorrelator is only capable of measuring the pulse duration to an accuracy of 4 fs. Since the difference in pulse duration between some of the on and off-axis measurements is less than this it may not be able to differentiate accurately enough to display the actual pulse duration at each point. Therefore, a measuring technique with an increased accuracy would have to be implemented in order to determine the actual value at different points through these lenses. A possible technique could be using Frequency-Resolved Optical Gating (FROG) [58] to measure the phase of the pulse but as it stands the data shows that there is no significant change in pulse duration between on and off-axis for these particular objective lenses since all data points fall within the same error range for every plot. This data agrees with the theoretical calculations carried out in Chapter 2.

3.6 Conclusion

The pulse duration was calculated to have increased from 130±4 fs to 190± fs for the 10x objective lens and from 146±5 fs to 353±8 fs for the 20x objective lens and therefore would benefit from employing a dispersion compensation technique to reduce or completely eliminate the pulse stretching. Similar to Chapter 2, no substantial change in pulse duration was measured for the output pulse duration through different points of the back aperture of the objective lens, with a change of less than 10 fs for both the 10x and 20x lenses. This in turn will not cause a notable problem during TPLSM since the output pulse duration has been measured to be almost identical at all points of the sample, which should create a homogenous image. The objective lenses used are standard for TPLSM. However, material dispersion might become increasingly problematic when using novel lenses such as the Mesolens discussed in Chapter 4, where there are many more internal elements with a much greater overall material thickness.

Chapter 4 - Extension of numerical model to mesocopic laser scanning microscopic objective

4.1 Introduction

The introduction of early optical microscopes revolutionised science providing the ability to produce two-dimensional images of three-dimensional samples. The microscope has constantly been redeveloped, introducing the likes of the familiar confocal microscope described previously [21] being capable of producing three-dimensional images. Historically such microscope lenses have focused solely on high resolution within a small image field [62].

Dr Brad Amos of the Laboratory of Molecular Biology, Cambridge and lens designer Mr Esmond Reid have now developed the Mesolens, which provides a much larger image field. The Mesolens has been designed to act like a magnifying glass, which is able to image the whole sample whilst simultaneously displaying the internal cell structures of the sample (Figure 25).

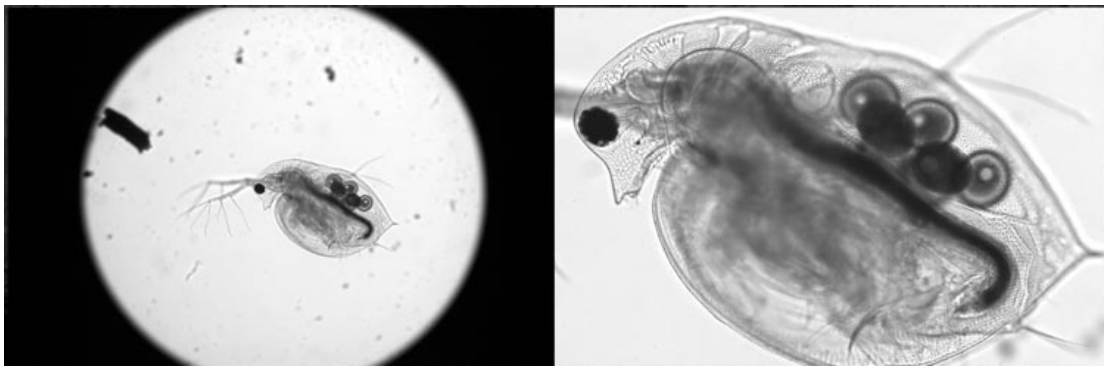

Figure 25 - An image taken of a living water flea (Daphnia) using the Mesolens, showing internal and external structures of the entire specimen in one go. The Daphnia is centred in the middle of the 6 mm diameter field of view of the Mesolens shown on the left alongside a close up shown on the right.

This allows scientists to see many thousands of cells at once but with a very high resolution than thought possible and a greatly improved perception of depth. This

new approach is intended to open many new possibilities in science and medicine having being developed in particular to examine genetically modified mouse embryos. Being able to do this will provide scientists with the ability to identify new treatments for illnesses, such as cases of cancer.

As discussed in previous chapters, we know that there are problems with temporal dispersion in TPLSM. The Mesolens has been developed for use with CLSM, however is currently being adapted for TPLSM. We have been provided with the exact design of this novel lens thanks to Brad Amos and Esmond Reid and therefore can calculate the pulse stretching on-axis by applying the previously shown numerical methods in Chapter 2. Off-axis measurements cannot be taken for the Mesolens because the image of the ray trace produced by Zemax is not accurate enough to measure off-axis thicknesses and therefore only on-axis pulse stretching will be considered.

4.2 Theory

The new lens is named the Mesolens to express similarities between the macrophotography lens and a microscopic objective lens, where the Mesolens covers the same area as the first lens and has as good a resolution as the second. Figure 26 shows an image taken using a conventional CLSM of a tropical freshwater fish known as a zebrafish to illustrate the requirement for the Mesolens.

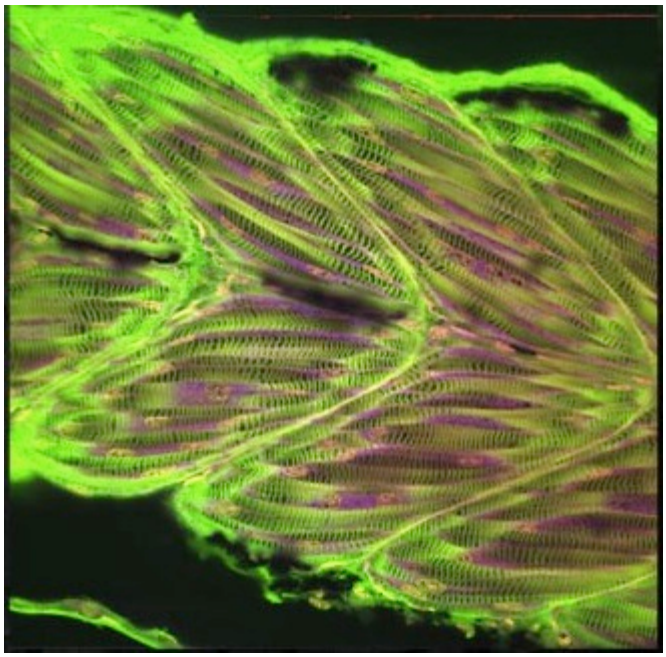

Figure 26 - Image taken from [63] of the tiny larva present in zebrafish using CLSM. The diameter of the larva shown is only 0.2mm across.

Despite the image being able to show precise structures within the zebrafish, it was only capable of imaging $1/5^{th}$ of a millimeter across the sample at any one time. The Mesolens was introduced to address this situation by providing a wider field of view but with the same high resolution.

For this novel lens to cover such a large sample area, the lens has to be large. It also has to have a low magnification of 4x and a high NA of 0.47, providing a higher spatial

resolution. Equation (43) describes the relationship between NA and the lateral resolution (r_{airy}), given in Chapter 1 [23].

$$r_{airy} = 0.61\frac{\lambda_0}{NA} \quad ...(43)$$

where r_{airy} refers to the radius of the first dark airy disk space surrounding the central disk of the diffraction image (Figure 27). The solution to Equation (43) is given as a measure of distance in the sample plane. The higher NA therefore decreases the distance between two resolving points of an image. Figure 27 displays the lateral resolution (r_{airy}), showing the resolution in two and three-dimensions of resolved, unresolved and resolution limited objects.

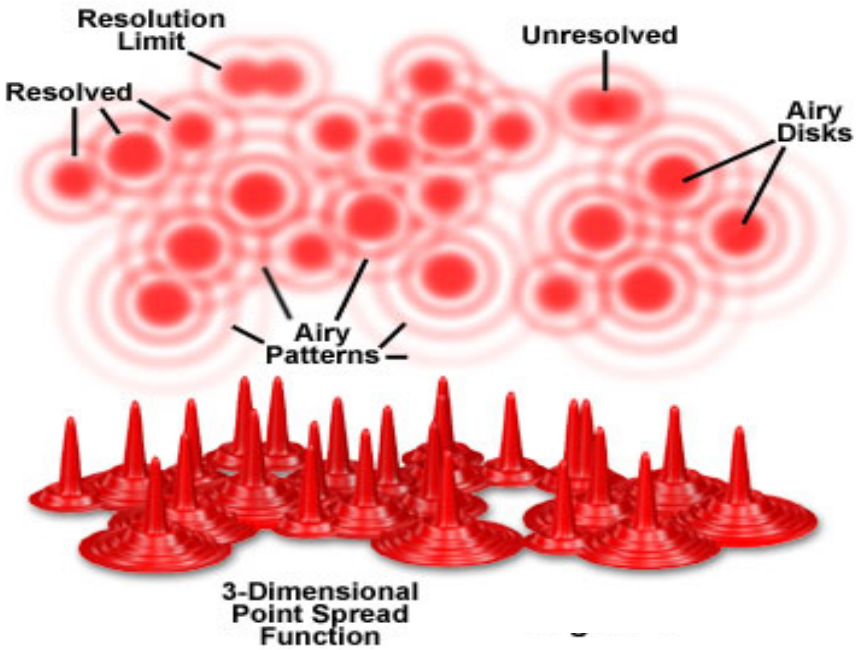

Figure 27 - Airy disk pattern and the limit of resolution [64].

The axial dimension is perpendicular to the lateral dimension and is given by [23]:

$$r_{axial} = \frac{2\lambda_0 n(\lambda)}{(NA)^2} \quad ...(44)$$

where n is the refractive index of the object medium. Again, in general terms this describes the resolution in terms of the distance between which two points can be resolved, but here in the z-direction.

The NA is proportional to the refractive index, n, and the half angle of the maximum cone of light that can enter the lens given by Equation (45).

$$NA = n\sin\theta \quad ...(45)$$

The large NA of the Mesolens therefore suggests a large half cone angle, which is the reason for the observed brightness of the images that are produced whilst using the lens [63].

To further illustrate the need for the Mesolens, the resolution for a standard objective lens of similar magnification will be compared to the Mesolens (Table 3). For a standard 4x objective lens the NA is often 0.1 [64]. The best lateral resolution for both lenses was calculated at a wavelength of 500 nm using the Abbe equation (Equation (44)) with the theoretical values displayed in Table 3.

	Magnification	NA	theoretical $r_{lateral}$(µm)	theoretical r_{axial}(µm)
Mesolens	4x	0.47	0.6	4
Nikon	4x	0.1	3	100

Table 3 - The lateral and axial resolution for the Mesolens compared to a standard Nikon objective lens.

Following this calculation the Mesolens has been calculated to provide a smaller lateral resolution and an improved axial resolution for better optical sectioning.

Figure 28 displays a human flea as seen through the new Mesolens, showing the flea in its entirety alongside Robert Hooke's drawing in his 1665*Micrographia* publication found in [65].

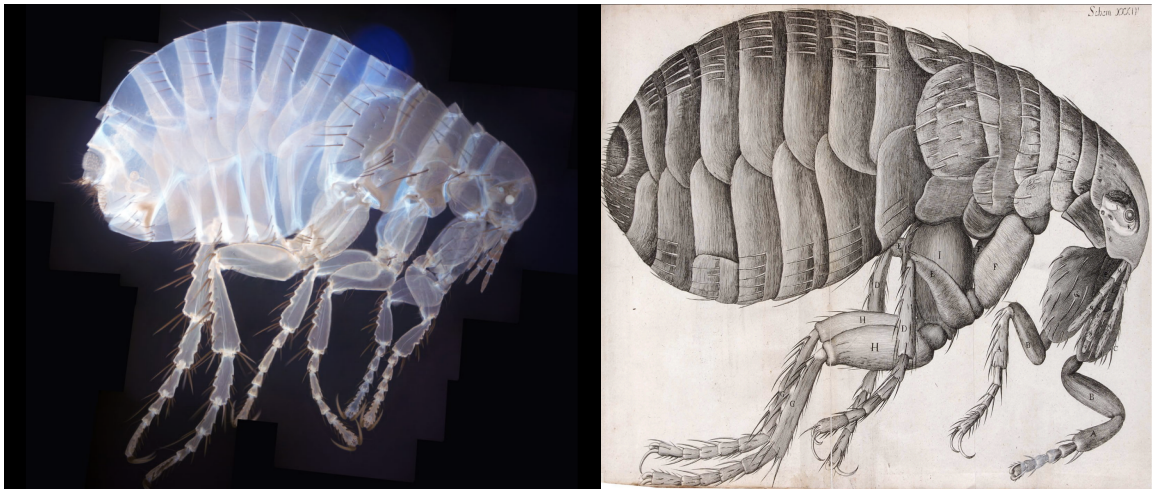

Figure 28 - Human flea as seen through the Mesolens (left) compared to Robert Hooke's engraving in his 1665 publication (right) [65].

The resolution of this image is 0.5 µm over the 6 mm diameter field, which requires a camera with 140 megapixels [64]. However, such a high megapixel camera was not available and therefore Figure 28 was comprised using a 14-megapixel Olympus PEN camera. Images were then obtained by translating the camera across the sample and stitching the images together using Photoshop. Another point to note is that Robert Hooke's version of a human flea was obtained using a tiny lens, which was made from a tiny bead of glass (approximately 1 mm in diameter). Dr Amos and his team have had to ignore this principle in the invention of the Mesolens since as mentioned in order to cover the large area that was required, they had to invent a large lens.

Having demonstrated the importance of the Mesolens in two dimensions, the next step is to explore the possibility of using the lens for three-dimensional imaging, using CLSM and TPLSM. However, as shown in previous chapters, even with small and modest objective lenses, a pulse duration of sub-200 fs can be significantly stretched at the sample stage. In this chapter, the implications of using such a large

lens for TPLSM will be analysed by again concentrating on the temporal dispersion. The change in the lens design will have an effect on the pulse duration at the sample plane as compared to a standard objective lens. Using the data for the Mesolens provided by Esmond Reid, the temporal dispersion was calculated through the Mesolens on-axis.

4.3 Methodology

In order to determine how much the pulse is stretched after propagating through the Mesolens the same method was carried out as previous for the generic objective lenses in Chapter 2. On-axis calculations were carried out first using the lens data for each individual element and again Equation (28), which was derived in Chapter 2 for the propagation of ultrashort pulses through a series of elements. To determine the most suitable input parameters to work with for this particular lens, the calculation was carried out for a range of wavelengths (λ = 700-960 nm) and input pulse durations (τ_0 = 1-500 fs), where Table 2 displays the calculated output pulse durations for different combinations of the two.

Using the output pulse durations calculated in Table 4, the probability of TPA was calculated using Equation (10) of chapter 1. Again, the two-photon cross sections of fluorescein was used [48] with an average power of 30 mW to produce the results shown in Figure 29.

4.4 Results

Using the previously derived equations (Chapter 2), the pulse stretching through this novel giant lens has been calculated using a combination of different wavelengths and initial input pulse durations, similar to the method used in Chapter 2 using the generic objective lenses.

Wavelength (nm)	1 fs	10 fs	50 fs	100 fs	140 fs	200 fs	500 fs
700	29400	2940	591	311	253	248	503
720	27800	2780	559	296	243	244	504
740	26200	2620	526	280	234	239	503
760	24400	2440	491	264	224	234	502
780	22500	2250	453	246	213	229	502
800	20400	2040	411	227	202	225	501
820	18000	1800	363	206	190	219	501
840	15700	1580	319	187	180	215	501
860	15700	1570	319	186	180	215	501
880	18640	1860	376	212	193	221	501
900	23100	2300	464	251	216	231	502
920	29400	2940	590	311	253	248	503
940	38700	3870	776	400	310	278	506
960	52700	5270	1056	537	402	331	511

Table 4 - put pulse duration after propagating through the Mesolens on-axis, using a varying combination of input pulse durations and wavelengths. The highlighted (in red) show the suggested best operating conditions, based on the two-photon absorption efficiency increasing at shorter pulse durations as per Equation (10).

The shortest output pulse durations are highlighted in red to display the combination of input pulse durations and wavelengths, which would be best to work with during TPLSM with the Mesolens. The output pulse durations displayed in Table 4 were used to calculate the corresponding probability of TPA for fluorescein and the results are displayed below in Figure 29.

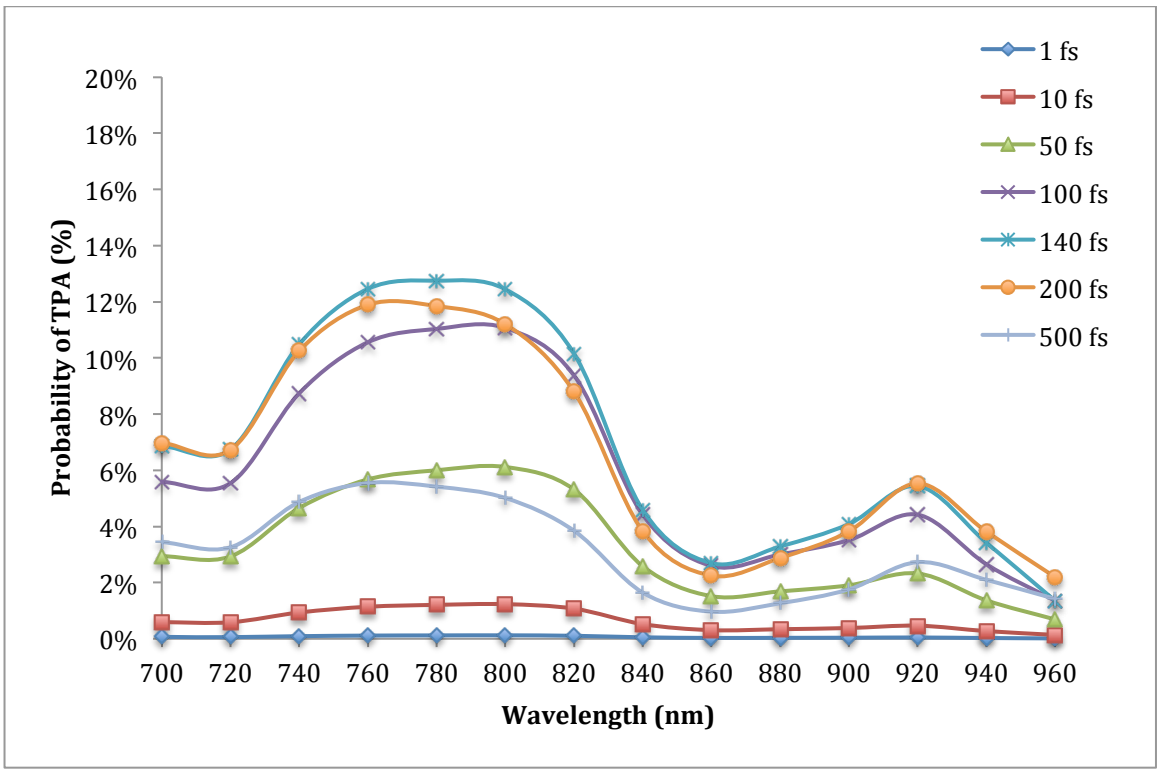

Figure 29 -The probability of TPA of fluorescein for the output pulse durations shown in Table 4 with an average power of 30 mW.

The same trend is seen as in Figures 12 and 13 of Chapter 2, however for this particular lens an input pulse duration of 140 fs at a wavelength of 780 nm has been calculated to produce the highest probability of TPA as opposed to 100 fs at a wavelength of 760 nm. This emphasizes the need to choose the input parameters carefully, where the highest probability of TPA can occur at different wavelengths and with different input pulse durations for different lenses.

4.5 Discussion

Comparing Table 1, 2 (Chapter 2) and Table 4 (this Chapter) for a pulse duration of 100 fs at a wavelength of 800 nm, the pulse was calculated to have stretched by 25 and 21 fs through a generic objective lens whereas it had stretched by 127 fs through the Mesolens. This large increase in pulse duration emphasizes the need for compensation. Off-axis measurements could not be made for this lens because the image of the traced rays using Zemax was not as accurate as hoped. However based on the previous calculations and measurements from Chapters 2 and 3 respectively there was shown to be little cause for concern. Although there is a significant increase in material dispersion for the Mesolens, the off-axis calculations for other cases have been shown to be relative to the on-axis and each has had a constant effect on the pulse duration across the back aperture of the objective lens. Therefore a reasonable assumption can be made that the Mesolens will have a similar effect upon the temporal dispersion off-axis as in the previous cases shown in Chapters 2 and 3.

When comparing Figure 12 and 13 (Chapter 2) and 26 (this chapter), the most striking difference was the highest percentage of TPA for each lens. In the case of the standard objective lens the highest probability of TPA was approximately 60% whereas for the Mesolens it was calculated to be as little as 14%. Both calculations have been calculated with identical parameters such as the fluorescein cross-section, average power etc. The only two parameters that were changed for the Mesolens were the pulse duration at the sample plane and the numerical aperture. By comparing these two figures it has shown the variation in the probability of TPA between different lenses. Choosing the most efficient input parameters for TPA is also highly important since when comparing Figures 12 and 29 the highest probability of TPA for fluorescein occurs at different wavelengths and with different initial pulse durations for two different lenses. Therefore carrying out the numerical simulation

shown in Chapter 2 for any lens can provide the necessary data to produce the highest probability of TPA before performing TPLSM.

4.6 Conclusion

The numerical simulation shown in Chapter 2 has been applied to a novel lens called the Mesolens, which has been developed to examine large tissue samples such as mouse embryos. It has been demonstrated that the Mesolens can produce a wider field of view by using a low magnification lens. The high NA has also been calculated to have an improved lateral and axial resolution compared to a standard 4x/0.1 NA objective lens. However, the limitation lies in the material dispersion as a result of using such a large lens, which as calculated can stretch a 100 fs pulse by as much as 127 fs. It was also calculated that the probability of TPA for the standard objective lenses was as much as 60% compared to 14% calculated for the Mesolens. This is a result of such high pulse stretching through the Mesolens compared to the standard objective lenses and therefore, the Mesolens would benefit from using a compensation technique. This will be discussed in more detail in Chapter 5.

Chapter 5 - Dispersion compensation: commercial objective lenses and Mesolens

5.1 Introduction

The effect of material dispersion upon ultrashort pulses has been discussed in detail throughout the previous Chapters and as mentioned, there is a great requirement for optical pulses to be short at the specimen plane, i.e. the objective lens focus [24]. This requires techniques to compensate for material dispersion present within the laser cavity and microscope optics, by providing anomalous dispersion. These techniques can include the use of prism pairs, photonic crystal fibre (PCF), diffraction gratings and often a combination of techniques [41]. In this particular study we will look into the theory of dispersion compensation by using a pair of diffraction gratings, which is a more useful technique being capable of working at any wavelength. In this chapter, the theoretical analysis of pulse stretching and compression will be presented using a numerical model to achieve a dispersion compensation technique that will reduce the pulse stretching caused by commercial objective lenses used in TPLSM and the Mesolens. In doing so it will maximize the probability of TPA, which as shown in Chapters 3 and 4 requires the shortest possible pulse at the sample plane.

5.2 Theory

5.2.1 Obtaining the total GVD for an entire objective lens

By rearranging the previous equations given in Chapter 2 it is possible to calculate the total normal GVD caused by an objective lens. In doing so, it is possible to introduce the correct quantity of anomalous dispersion using a grating pair to cancel the normal dispersion caused by the objective lens. Firstly, the GVD dispersion for each individual element can be found using Equation (7) in Chapter 1. By referring back to Equation (28) of Chapter 2 it is possible to rewrite this equation to find the total GVD for one objective lens, $\beta_{2,\,tot}$:

$$\frac{z_{tot}\left|\beta_{2,tot}\right|}{\tau_0^2} = \sum_{m=1}^{\infty}\left(\frac{z_m\left|\beta_{2,m}\right|}{\tau_0^2}\right) \quad \ldots(46)$$

where z_{tot} is the total thickness of the internal elements. Equation (46) can then be rearranged further producing:

$$\left|\beta_{2,tot}\right| = \sum_{m=1}^{\infty}\left(\frac{z_m\left|\beta_{2,m}\right|}{\tau_0^2}\right)\frac{\tau_0^2}{z_{tot}} \quad \ldots(47)$$

Using the details for the cytometry lens, Nikon objective lens (Chapter 2) and the Mesolens (Chapter 4), the dispersion of each lens can be calculated, and hence the amount of negative dispersion required can be determined.

5.2.2 Diffraction gratings for pulse compression

As well as GVD, optical pulses can also gain chirping from self-phase modulation (SPM), which is a result of the Kerr nonlinearity of the gain medium within the laser cavity. Optical pulses produced by mode-locked lasers utilize a balance of both SPM and GVD to produce stable operation known as soliton mode-locking and both are used to compress optical pulses in the likes of single-mode fibers [66]. The Ti:Sapphire laser exhibits normal dispersion where longer wavelengths travel faster than short, which as mentioned causes temporal spreading of the pulse. This occurs on each trip through the laser cavity every time it passes through the Ti:Sapphire crystal or as it travels through other material such as objective lenses [36]. Dispersion compensation must be put in place to overcome both GVD and SPM since a pulse oscillating back and forth will gain a small chirp from any number of the dispersive materials within the laser cavity or optical elements. Many designs have been implemented to reduce the GVD present in lasers such as the Brewster prism pair, which is contained within the Ti:Sapphire cavity, and even a four-prism sequence [41]. In order to produce the required ultrashort pulses a method of anomalous dispersion should be implemented into the cavity to compensate for the normal dispersion caused by the laser crystal itself or in this case the objective lens.

5.2.2.1 Theoretical model

Having derived and discussed a suitable model to quantify the normal dispersion introduced by an objective lens, it is now required to calculate the anomalous dispersion introduced by a grating pair. When a spectrally broad laser pulse is incident upon a diffraction grating the component wavelengths (or frequencies) will each diffract at various angles (θ_2), which are wavelength dependent given by the grating equation [67]:

$$\Lambda(\sin\theta_i + \sin\theta_r) = n\lambda \quad ...(48)$$

where Λ is the grating period, θ_i and θ_r are respectively the angles of the incident and diffracted light relative to the grating, n is an integer and λ is the wavelength of light. This equation describes the path taken for each individual wavelength, where the leading edge of the pulse (higher wavelengths) will be diffracted at a larger angle and the trailing edge of the pulse (shorter wavelengths) will be diffracted at a smaller angle. Placing a second diffraction grating some separation distance, l, from the first then causes the pulse to collimate, producing a stretched pulse with all frequency components travelling at the same speed.

Following Agrawal [11] the effective anomalous dispersion required to compress ultrashort pulses will be derived. Figure 30 illustrates the geometry of a pair of gratings, and the incident and diffracted beams.

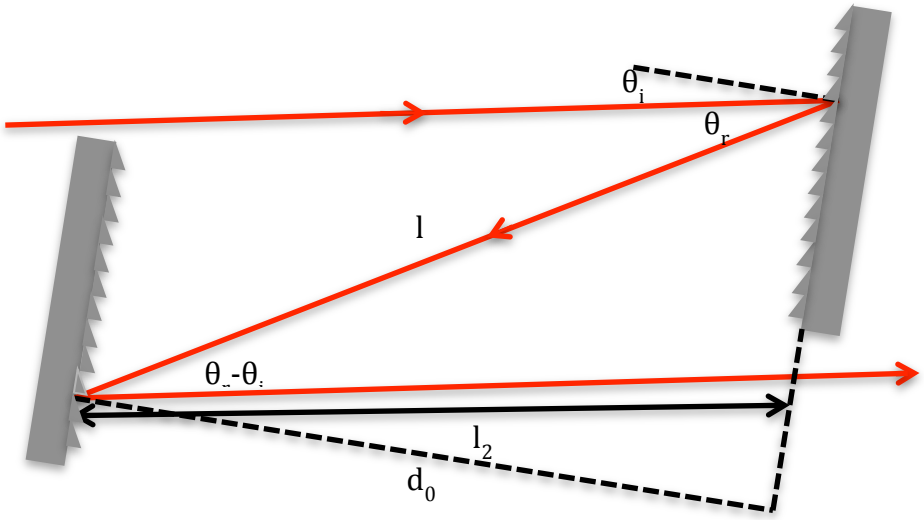

Figure 30 – Diagram illustrating the geometry for a pair of diffraction gratings.

In order to determine the wavelength dependent angle of diffraction, Equation (48) can be rearranged to produce:

$$\sin\theta_r = \frac{\lambda}{\Lambda} - \sin\theta_i \quad ...(49)$$

The time delay introduced by the diffraction gratings is also wavelength dependent and is given by:

$$t_d = \frac{l(\omega)}{c} = \frac{d\phi_c}{d\omega} \quad ...(50)$$

This equation is simply the rearrangement of one of the kinematic equations where the length (l(ω)) is the total path length (l_1+l_2) from Figure 30 and ϕ_c is the phase shift. The total path length can be calculated geometrically from the schematic diagram (Figure 30) using Pythagoras theorem and is given by Equation (51) below.

$$l(\omega) = l_1 + l_2 = d_0 \frac{\cos(\theta_r - \theta_i)}{\cos(\theta_r)} \quad ...(51)$$

In order to determine the GVD effects related to the grating pair the phase shift is expanded around the centre frequency (ω_0) shown in Equation (52).

$$\phi_c(\omega) = \phi_0 + t_c(\omega - \omega_0) - a_c(\omega - \omega_0)^2 + b_c(\omega - \omega_0)^3 + \ldots (52)$$

where ϕ_0 is a constant, t_c is a constant time delay and a_c and b_c are the second and third order GVD effects associated with the grating pair. For this study only second order effects are being analysed and therefore only the effect of a_c upon the phase shift is required and can dismiss the constants and other linear terms to become:

$$\phi_c(\omega) = -a_c(\omega - \omega_0)^2 \ldots (53)$$

where a_c is the second order GVD parameter, which is associated with the grating pair given by Equation (54) and b_0 is the centre-to-centre spacing between the gratings.

$$a_c = \frac{4\pi^2 c b_0}{\omega_0^3 \Lambda^2 \cos^2\theta} \ldots (54)$$

where c is the speed of light (ms^{-1}), ω_0 is the frequency of the pulse (Hz), Λ is the grating period (m^{-1}) and θ is the angle of first order diffraction. since it has a positive value the phase shift is negative and is therefore termed anomalous dispersion. The centre-to-centre spacing term (b_0) is given by:

$$b_0 = d_0 \sec\theta_{r,0} \ldots (55)$$

where d_0 is the grating separation as illustrated in Figure 30. To fully understand the anomalous GVD associated with a diffraction pair it is useful to study the optical field at the output end of the grating pair given by:

$$U_{out}(T) = \frac{1}{2\pi}\int_{-\infty}^{\infty}\tilde{U}_{in}(\omega-\omega_0)\exp\left[i\phi_c(\omega)-i\omega T\right]d\omega \quad ...(56)$$

where $\tilde{U}_{in}(\omega)$ is the Fourier transform of the input field. Since equation (56) is described in a similar approach as equation (20) of Chapter 2 the effective anomalous dispersion introduced by a pair of diffraction gratings can be calculated using Equation (57) [11].

$$\beta_2^{eff} = \frac{-2a_c}{b_0} \quad ...(57)$$

Altering the line spacing and grating separation to produce an equal and opposite value for β_2 will ultimately compensate for the material dispersion present within any microscope objective lens and produce the original pulse duration at the sample plane. Following this series of equations, a useful method of calculating the effective GVD provided by diffraction gratings can be calculated and a suitable value for the different input parameters can then be determined depending on the quantity of positive material dispersion introduced by an objective lens

5.3 Results of calculation

The total GVD introduced by the 10x cytometry lens, the 20x Nikon objective lens and the Mesolens was calculated using Equation (47) with the corresponding values shown in Table 5.

Lens	β_2 (ps^2/m)
Cytometry	5.78×10^{-2}
Nikon	7.82×10^{-2}
Mesolens	1.05×10^{-1}

Table 5 – The GVD calculated for each lens at a wavelength of 800nm.

Using Equation (57) the effective GVD introduced by a grating pair was calculated at a wavelength of 800 nm. Table 6 displays the results with a different combination of input parameters for the grating separation and the number of lines/mm.

β2 with a line separation (lines/mm) of….				
Grating separation	300	600	900	1200
5mm	-8.93×10^{-4}	-4.83×10^{-3}	-2.20×10^{-2}	-5.94×10^{-1}
7mm	-1.25×10^{-3}	-6.77×10^{-3}	-3.07×10^{-2}	-8.32×10^{-1}
10mm	-1.79×10^{-3}	-9.67×10^{-3}	-4.39×10^{-2}	-1.19×10^{0}
20mm	-3.57×10^{-3}	-1.93×10^{-2}	-8.78×10^{-2}	-2.38×10^{0}
25mm	-4.47×10^{-3}	-2.42×10^{-2}	-1.10×10^{-1}	-2.97×10^{0}
50mm	-8.93×10^{-3}	-4.83×10^{-2}	-2.20×10^{-1}	-5.94×10^{0}
75mm	-1.34×10^{-2}	-7.25×10^{-2}	-3.29×10^{-1}	-8.92×10^{0}
100mm	-1.79×10^{-2}	-9.67×10^{-2}	-4.39×10^{-1}	-11.9×10^{0}
200mm	-3.57×10^{-2}	-1.93×10^{-1}	-8.78×10^{-1}	-23.8×10^{0}

Table 6 – The value for β (ps^2/m) when using different input parameters for the grating spacing and lines/mm at a wavelength of 800 nm. The angle of incidence was assumed to be zero. The highlighted results show the suggested operating conditions, based on Equation (57) for the cytometry (blue), Nikon (green) and Mesolens (red) to reduce GVD.

Other values were obtained between a wavelength range of 700-900 nm (Appendix 5), however no significant variation in the effective GVD was calculated. Therefore, assuming a wavelength of 800 nm sensible input parameters to compensate for material dispersion for each of the three lenses has been selected from Table 6. The grating and line separation that could compensate for the normal dispersion in the cytometry lens, Nikon lens and Mesolens could be 900 lines/mm separated by 10mm, 600 lines/mm separated by 75mm and 900 lines/mm separated by 25mm respectively.

5.4 Discussion

The theory of compensating for ultrashort pulse stretching has been analysed using a grating pair. Using this particular method, an accurate calculation for the GVD which can be introduced into an optical system to compensate for pulse stretching through three previously discussed lenses has been carried out, the cytometry and Nikon lenses used in Chapter 2 and the novel Mesolens discussed in Chapter 4. These particular lenses were used, since in the previous chapters all necessary parameters were calculated or were previously provided by the manufacturer. The line spacing and grating separation that could be used to compensate for the material dispersion for these three particular lenses has been highlighted in Table 6, however as can be seen that there are a couple of other combinations of line and grating separation that could also be used to compensate for normal dispersion. For example, the pulse stretching through the Mesolens could be compensated for using a grating pair with a separation distance of 25 mm and a line spacing of 900 lines/mm or 200 mm with a line spacing of 600 lines/mm. However, there is a practical issue involved in deciding the most appropriate parameters to use. With all the other optical elements within a microscope it becomes more practical to use smaller grating separations. Diffraction gratings with lower line spacing is commercially available and are used in dispersion compensation studies [67], however for the lenses being analysed in this study they were not required and therefore the lowest line spacing analysed was 1200 lines/mm.

5.5 Conclusion

It has been theoretically demonstrated that a pair of diffraction gratings can be used to compress stretched laser pulses by introducing the correct quantity of anomalous dispersion. This would be a fairly easy experiment to set-up, by placing the diffraction gratings before the objective lens, with a separation distance that can be calculated using the methods discussed. This Chapter has demonstrated an accurate method to compensate for large amounts of second-order dispersion caused by the novel Mesolens by using a grating pair of 900 lines/mm separated by a distance of 25 mm. This shows that using a large lens necessary to cover such large sample areas does not generate any uncontrollable quantities of normal dispersion.

Chapter 6 – Conclusion

6.1 Summary of thesis

As discussed in Chapter 1, material dispersion has an overall effect on the duration of ultrashort pulses used in TPLSM where ultrashort pulses are required for a higher probability of TPA [20]. In this thesis the temporal dispersion introduced by microscope objective lenses on ultrashort pulses has been quantified using a series of Equations discussed extensively throughout.

The manufacturer, due to confidentiality agreements, almost never provides the objective lens data. Therefore, to begin with, two generic objective lenses of different magnification that were provided with the lens data were obtained from US Patents [7], [8] to illustrate the magnitude of the pulse stretching through a 10x/1.2 NA cytometry lens and a 20x/0.75 NA Nikon objective lens. For on axis calculations with an initial pulse duration of 100 fs at a wavelength of 800 nm the cytometry lens displayed an increase of 21 fs and the Nikon lens displayed a smaller increase of 25 fs. Since the laser beam scans the back of an objective lens during LSM off-axis measurements were also obtained for the 20x Nikon lens, which was calculated to have sub-fs changes in the pulse duration. This is not a concerning change in the output pulse duration and therefore can be considered negligible since the current optical electronic measuring devices can only measure as accurate as a few fs.

The increase in pulse duration through a 10x/0.45 NA Nikon lens and a 20x/0.75 NA Nikon lens was experimentally demonstrated in Chapter 3, which again displayed no substantial change in off-axis pulse durations, with less than a 10 fs change for both. However for the 10x objective lens material dispersion caused the pulse duration to increase from 130±4 fs to 190±5 fs and the 20x objective lens was increased from 146±5 fs to 353±8 fs. By referring to both Chapter 2 and 3 it has been shown that TPLSM can be confidently obtained knowing that the effect of off-axis pulse propagation will cause no significant effect on the probability of TPA and hence the image resolution.

Chapter 4 involved applying the theory presented in the previous chapters to a novel lens known as the Mesolens, which has been introduced to image a wider field of view. To image such a large area the lens had to be large, which therefore suggested that this would result in an increased effect of temporal dispersion since the overall thickness of material compared to the commercial lenses was larger. It was possible to quantify this effect using the previously derived equations along with the lens data provided by the lens designer. It was calculated that a 100 fs pulse at a wavelength of 800 nm increased by as much as 127 fs.

In Chapters 2 and 4 the probability of TPA was plotted as a function of wavelength for different initial pulse durations using the data obtained from the cytometry, Nikon and Mesolens. As expected the highest probability of TPA for the Mesolens was significantly lower than that of the Nikon lens for the same average power. The highest probability for the Mesolens was only 13% (780 nm 140 fs) and for the Nikon it was as high as 73% (760 nm 100 fs). This reduction in TPA was expected because of the larger quantity of material and as a result the Mesolens was shown to benefit from using a compensation technique as discussed in Chapter 5.

Having discussed the effect of material dispersion on ultrashort pulses Chapter 5 demonstrated an accurate method of compensating for the large quantities of dispersion introduced by the commercial lenses discussed in Chapter 2 and in particular the Mesolens discussed in Chapter 4. By using a grating pair of 900 lines/mm separated by a distance of 25 mm it was calculated to introduce $-1.10\text{x}10^{-1}$ ps^2/m of anomalous dispersion to compensate for the $1.05\text{x}10^{-1}$ ps^2/m of normal dispersion. This demonstrated that it was possible to control large quantities of normal dispersion by simply using a diffraction grating pair that can be easily be inserted before the objective lens of a microscope.

As shown, the objective of this study has been fulfilled having demonstrated numerical methods of calculating and measuring the temporal dispersion of lenses of known and unknown internal elements. The novelty of this study is in applying the calculation to a completely new lens that has been designed to have a large field of view and as a result limits the use of the shortest possible pulse durations. Therefore

a compensation technique using a grating pair has been shown to apply the correct quantity of anomalous dispersion to compensate for the normal dispersion introduced while propagating through the lens.

References

[1] M. Oheim, E. Beaurepaire, E. Chaigneau, J. Mertz, and S. Charpak, “Two-photon microscopy in brain tissue : parameters influencing the imaging depth,” *Journal of Neuroscience Methods*, vol. 111, pp. 29 - 37, 2001.

[2] M. J. Levene et al., “In Vivo Multiphoton Microscopy of Deep Brain Tissue In Vivo Multiphoton Microscopy of Deep Brain Tissue,” *Journal of Neurophysiology*, no. 2003, pp. 1908-1912, 2011.

[3] P. T. C. Masters, Barry R & So, *The Handbook of BIOMEDICAL NONLINEAR OPTICAL MICROSCOPY*. Oxford University Press, Inc, 2008, p. 457.

[4] P. T. C. Masters, Barry R & So, *Handbook of BIOMEDICAL NONLINEAR OPTICAL MICROSCOPY*. 2008, p. 106.

[5] A. Jesacher, S. Bernet, and M. Ritsch-Marte, “Spiral phase contrast imaging in microscopy,” *Optics Express*, vol. 13, no. 3, pp. 689-694, 2005.

[6] J. B. Guild, C. Xu, and W. W. Webb, “Measurement of group delay dispersion of high numerical aperture objective lenses using two-photon excited fluorescence,” *Applied Optics*, vol. 36, no. 1, pp. 397-401, 1997.

[7] B. J. Blasenheim, “Flow Cytometry Lens System,” U.S. Patent US 6,510,0072003.

[8] I. Ito, “Microscope objective lens,” U.S. Patent 5,729,391 (1998).

[9] W. R. Zipfel, R. M. Williams, and W. W. Webb, “Nonlinear magic : multiphoton microscopy in the biosciences,” *Nature Biotechnology*, vol. 21, no. 11, pp. 1369-1377, 2003.

[10] Knowledge at FiberOptic.com, “Chromatic Dispersion (optics).” [Online]. Available At: http://www.fiberoptic.com/Fiber_Characterization/pdf/chromatic_dispersion.pdf. [Accessed: 02-Nov-2011].

[11] G. P. Agrawal, *Nonlinear fiber optics*. Academic Press, 1989.

[12] Schott, “Inquiry Glass Overview Excel Table.” [Online]. Available At: http://www.schott.com/advanced_optics/english/our_products/materials/data_tools/index.html?so=uk&lang=english. [Accessed: 08-Sep-2011].

[13] G. Ghosh, M. Endo, and T. Iwasalu, “Temperature-Dependent Sellmeier Coefficients and Chromatic Dispersions for Some Optical Fiber Glasses,” *Lightwave*, vol. 12, no. 8, pp. 1338-1342, 1994.

[14] E. R. Brown et.al., “State of the art in 1.55 micrometer ultrafast InGaAs photoconductors, and the use of signal-processing techniques to extract photocarrier lifetime,” *Semicond. Sci. Technol*, vol. 20, no. 7, 2005.

[15] OHARA, “Optical Properties,” *Ohara Corporation*. [Online]. Available At: http://www.oharacorp.com/o2.html. [Accessed: 06-Oct-2011].

[16] N. C. Bruce and C. J. Rom, “Calculation of temporal spreading of ultrashort pulses propagating through optical glasses,” *Revista Mexicana De Fisica*, vol. 54, pp. 141-148, 2008.

[17] Jenkins and White, *Dispersion in Fundamentals of Optics*, Second Edi. McGraw-Hill, 1951.

[18] T. Matsuda, Y. Funae, M. Yoshida, T. Yamamoto, and T. Takaya, “Optical Material of High Refractive Index Resin Composed of Sulfur-Containing Aliphatic and Alicyclic Methacrylates,” *Polymer*, vol. 76, no. 1999, pp. 45- 49, 2000.

[19] “Refractive Index.info.” [Online]. Available At: http://refractiveindex.info/?group=SCHOTT&material=N-BK7. [Accessed: 18-Oct-2011].

[20] W. Wang, Y. Liu, P. Xi, and Q. Ren, “Origin and effect of high-order dispersion in ultrashort pulse multiphoton microscopy in the 10 fs regime,” *Applied Optics*, vol. 49, no. 35, pp. 6703-6709, 2010.

[21] J. B. Pawley, *Handbook of biological confocal microscopy*. Springer Verlag, 2006.

[22] C. R. Blanchard, “Atomic Force Microscopy,” *The Chemical Educator*, vol. 1, no. 5, pp. 1-8, 1996.

[23] J. B. Pawley, *Handbook of Biological Confocal Microscopy*, Third Edition. Springer, 2006, pp. 36-41.

[24] D. Semwogerere and E. R. Weeks, “Confocal Microscopy,” *Biomedical Engineering*, 2005.

[25] S. W. Paddock, T. J. Fellers, and M. W. Davidson, “Nikon MICROSCOPY.” [Online]. Available At: http://www.microscopyu.com/articles/confocal/confocalintropreparation.html. [Accessed: 17-Oct-2011].

[26] D. M. Shotton, “Confocal scanning optical microscopy and its applications for biological specimens,” *Journal of Cell Science*, vol. 94, pp. 175-206, 1989.

[27] J. Korlach, P. Schwille, W. W. Webb, and G. W. Feigenson, “Characterization of lipid bilayer phases by confocal microscopy and fluorescence correlation spectroscopy.,” *Proceedings of the National Academy of Sciences of the United States of America*, vol. 96, no. 15, pp. 8461-6, Jul. 1999.

[28] M. Rajadhyaksha and et al, “In Vivo Confocal Scanning Laser Microscopy of Human Skin: Melanin Provides Strong Contrast,” *Journal of Investigative Dermatology*, vol. 104, pp. 946-952.

[29] A. Richter-Dahlfors and et al, “Murine Salmonellosis Studied by Confocal Microscopy: Salmonella typhimurium Resides Intracellularly Inside Macrophages and Exerts a Cytotoxic Effect on Phagocytes In Vivo,” *The Journal of Experimental Medicine*, vol. 186, no. 4, pp. 569-580, 1997.

[30] D. Cutchey, “Multiphoton Microscopy,” *Imaging & Microscopy*, vol. 13, no. 3, pp. 50-51, 2011.

[31] A. Ustione and D. W. Piston, “A simple introduction to multiphoton microscopy,” *Journal of Microscopy*, vol. 243, no. June, pp. 221-226, 2011.

[32] F. Helmchen and W. Denk, “Deep tissue two-photon microscopy,” *Nature Methods*, vol. 2, no. 12, 2005.

[33] D. L. Spector and R. D. Goldman, *Basic Methods in Microscopy*. New York: Gold Spring Harbor Laboratory Press, 2006.

[34] I. Gryczynski, H. Malak, and J. R. Lakowicz, “Three-photon induced fluorescence of 2,5-diphenyloxazole with a femtosecond Ti:sapphire laser,” *Chemical Physics Letters*, vol. 2614, no. 95, pp. 1-6, 1995.

[35] H.-J. Wei, D. Xing, H.-M. Gu, Y. Jin, and X.-Y. Li, “Differences in optical properties between healthy and pathological human colon tissues using a Ti:sapphire laser: an in vitro study using the Monte Carlo inversion technique,” *Journal of Biomedical Opt.*, vol. 10, 2005.

[36] Coherent Ltd, “Operator’s Manual, The Coherent Mira Model 900-F Laser.” 2011 version .

[37] J. Wilson and J. F. B. Hawkes, *Lasers, Principles and Applications*. Prentice Hall Europe, 1987.

[38] D. Armstrong, “Ultrafast Lasers for Microscopy: Flexibility Plus State-of-the-Art Performance,” *bio PHOTONICS*, 2011. [Online]. Available: http://www.photonics.com/Article.aspx?AID=45698. [Accessed: 29-Sep-2011].

[39] M. Kempe and W. Rudolph, “Femtosecond pulses in the focal region of leses,” *Physical Review A*, vol. 48, no. 6, 1993.

[40] W. Denk, J. P. Strickler, and W. W. Webb, “Two-Photon Laser Scanning Fluorescence Microscopy,” *Biopolymers*, no. April, pp. 1-4, 1990.

[41] G. Mcconnell and E. Riis, “Ultra-short pulse compression using photonic crystal fibre,” *Applied Physics B*, vol. 563, pp. 557-563, 2004.

[42] I. D. Jung and F. X. K, “Self-starting 6 . 5-fs pulses from a Ti : sapphire laser,” *Optics Letters*, vol. 22, no. 13, pp. 1009-1011, 1997.

[43] U. Keller and J. E. Cunningham, “Femtosecond pulses from a continuously self-starting passively mode-locked Ti:sapphire laser,” *Optics Letters*, vol. 16, no. 13, pp. 1022-1024, 1991.

[44] M. S. Pshenichnikov, W. P. D. Boeij, and D. A. Wiersma, “Generation of 13-fs, 5-MW pulses from a cavity-dumped Ti:Sapphire laser,” *Optics Letters*, vol. 19, no. 8, pp. 572-574, 1994.

[45] M. Y. Hamza, S. Tariq, and A. F. Loss, “Split Step Fourier Method Based Pulse Propagation Model for Nonlinear Fiber Optics,” *Electrical Engineering*, pp. 1-5, 2007.

[46] SYNOPS, “CODE V Optical Design Software,” *Optical Research Associates*. [Online]. Available At: http://www.opticalres.com/. [Accessed: 29-Sep-2011].

[47] J. Bewersdorf, S. W. Hell, H. Resolution, O. Microscopy, and M.-planck-institute B. Chemistry, “Picosecond pulsed two-photon imaging with repetition rates of 200 and 400 MHz,” *Microscopy*, vol. 191, no. July, pp. 28-38, 1998.

[48] M. A. Albota, C. Xu, and W. W. Webb, “Two-photon fluorescence excitation cross sections of biomolecular probes from 690 to 960 nm,” *Applied Optics*, vol. 37, pp. 1-5, 1998.

[49] APE, “Your Partner in Ultrafast,” 2010. [Online]. Available At: http://www.ape-berlin.de/gb/produkte/PulseCheck.html. [Accessed: 10-Sep-2011].

[50] C. Xu and W. W. Webb, “Measurement of two-photon excitation cross sections of molecular fluorophores with data from 690 to 1050 nm,” *J. Opt. Soc. Am B*, vol. 13, no. 3, pp. 481-491, 1996.

[51] F. L. Pedrotti and et.al., *Introduction to optics*, 3rd ed. Pearson Prentice Hall, 2007, pp. 131-223.

[52] A. Yariv, *Optical Electronics in Modern Communications*, Fifth. Oxford University Press, Inc, 1997, pp. 203-206.

[53] K. Shimoda, “Introduction to Laser Physics,” *Optical Sciences*, vol. 44, p. 222, 1984.

[54] F. Krausz, “Kerr lens mode locking,” *Optics Letters*, vol. 17, no. 18, pp. 1292-1294, 1992.

[55] J. Herrmann, “Theory of Kerr-lens mode locking : role of self-focusing and radially varying gain,” *J. Opt. Soc. Am B*, vol. 11, no. 3, pp. 498-512, 1994.

[56] C. Antoncini, “Ultrashort laser pulses.” [Online]. Available At: http://www.ull.rdg.ac.uk/documents/ULL_Antoncini.pdf. [Accessed: 02-Nov-2011].

[57] J. P. Zheng, K. L. Jiao, and W. P. Shen, “Highly sensitive photodetector using porous silicon,” *Applied Physics Letters*, vol. 61, pp. 459-461, 1992.

[58] R. Trebino, “The Measurement of Ultrashort Laser Pulses.” [Online]. Available At: http://frog.gatech.edu/UFOBook/06-Pulse-measurement-Trebino.pdf. [Accessed: 05-Aug-2011].

[59] R. Trebino and D. J. Kane, “Using phase retrieval to measure the intensity and phase of ultrashort pulses : frequency-resolved optical gating,” *J. Opt. Soc. Am B*, vol. 10, no. 5, pp. 1101-1111, 1993.

[60] G. Taft et al., “Ultrashort optical waveform measurements using frequency-resolved optical gating,” *Optics Letters*, vol. 20, no. 7, pp. 743-745, 1995.

[61] R. P. Lucht, “Femtosecond Lasers for Molecular Measurements,” *Science*, vol. 316, no. 2007, pp. 207-208, 2007.

[62] S. B. Ippolito, B. B. Goldberg, and M. S. Ünlü, “High spatial resolution subsurface microscopy High spatial resolution subsurface microscopy,” *Applied Physics Letters*, vol. 4071, no. 2001, pp. 1-4, 2011.

[63] B. Amos, E. Reid, and S. Reichelt, “Mesolens,” 2011. [Online]. Available At: http://www2.mrc-lmb.cam.ac.uk/newgiantlens/index.html. [Accessed: 12-Oct-2011].

[64] K. R. Spring and M. W. Davidson, “Nikon MICROSCOPY.” [Online]. Available At: http://www.microscopyu.com/articles/optics/objectiveproperties.html. [Accessed: 12-Oct-2011].

[65] F. Barnard and R. B. Librarian, “Micrographia Special Collections featured item for March 2008 by,” *Reading*, 2008. [Online]. Available At: http://www.henleymba.com.hk/web/FILES/special-collections/featuremicrographia.pdf. [Accessed: 10-Oct-2011].

[66] W. J. Tomlinson, R. H. Stolen, and C. V. Shank, “Compression of optical pulses chirped by self-phase modulation in fibers,” *J. Opt. Soc. Am B*, vol. 1, no. 2, pp. 139-149, 1984.

[67] S. Kane, J. Squier, J. V. Rudd, and G. Mourou, “Hybrid grating-prism stretcher-compressor system with cubic phase and wavelength tunability and decreased alignment sensitivity,” *Optics Letters*, vol. 19, no. 22, pp. 1876-1878, 2000.

Appendices

Appendix 1 – Optical elements in cytometry lens

Surface	Thickness (mm)	Material
OBJ	0.0889	Water
1	1.94	Silica
2	0.1682	Gel
3	0.8	BK7
4	3.915	BK7
5 (AST)	1.5	Air
6	5	BK7
7	1	Air
8	5	BK7
9	1	Air
10	9	BK7
11	3	SF8
12	2	Air
13	3	SF8
14	12	BK7
15	126.731	Air

Table 7- Refractive surfaces, thicknesses and material of each of the lens elements, which comprise the objective cytometry lens displayed in Figure 8 [7].

Appendix 2 – Calculation for the pulse stretching through cytometry lens

When calculating the increase in pulse duration through a generic objective lens (cytometry lens) the following calculation was carried out using the data in Table 8 (Appendix 1). The material of each individual element was provided and the corresponding Sellmeier co-efficients below were used to find the second derivative of the refractive index at a wavelength of 800 nm.

	Material Name…		
Sellmeier Coefficient	BK7	SF8	FUSED SILICA
B1	1.03961212	1.55075812	0.6961663
B2	0.231792344	0.209816918	0.4079426
B3	1.01046945	1.46205491	0.8974794
C1	0.006000699	0.011433834	0.004679148
C2	0.020017914	0.058272565	0.013512063
C3	103.560653	133.24165	97.9340025

Table 8 – Sellmeier co-efficients for the lens material in the cytometry lens.

To begin with, the second derivative of the refractive index was calculated for each element with the corresponding values shown in the second column of Table 9. Using Equation (11) and the second derivatives of the refractive indices in Table 9 the group velocity dispersion, β_2, was calculated for element 1 as follows:

$$\beta_2 = \frac{\lambda_0^3}{2\pi c^2}\frac{d^2 n}{d\lambda^2}$$

$$\beta_2 = \frac{\left(800\times10^{-9}\right)^3}{2\times\pi\times(3\times10^8)^2}\times 4.95\times10^{10}$$

$$\beta_2 = 0.045 ps^2/m$$

The group velocity dispersion values calculated in the same way for the rest of the elements are given in the third column of Table 9.

In order to calculate the dispersive length the actual pulse duration must be calculated by dividing 100 fs by 1.665 ensuring that the initial pulse duration is consistent with a $sech^2$ pulse, according to Equation (28) in Chapter 2. This gives an initial pulse duration of 0.06 ps. Using Equation (12) and β_2, which was calculated previously the dispersive length L_D was calculated for the first element as follows:

$$L_D = \frac{\tau_0^2}{|\beta_2|}$$

$$L_D = \frac{(0.06)^2}{|0.045|}$$

$$L_D = 0.08m$$

The remainder of the values for the other elements is shown in the fourth column of Table 10 below.

Element No.	$d^2n/d\lambda^2$	$\beta_2(ps^2/m)$	L_D
1	$4.95x10^{10}$	0.045	0.08
2	$1.49x10^{11}$	0.135	0.027
3	$1.49x10^{11}$	0.135	0.027
4	$4.95x10^{10}$	0.045	0.08
5	$4.95x10^{10}$	0.045	0.08
6	$4.95x10^{10}$	0.045	0.08
7	$4.95x10^{10}$	0.045	0.08
8	$4.95x10^{10}$	0.045	0.08
9	$4.01x10^{10}$	0.036	0.1

Table 9 – Calculated values of the second order refractive index, the dispersion parameter and the dispersive length for each element in the cytometry lens.

As described in Equation (11), the output pulse duration depends on the sum of the length of material through which the pulse propagates divided by the dispersive length. Using the dispersive lengths calculated in Table 9 along with the corresponding material thicknesses from Table 8 of Appendix 1, the output pulse duration for a 100 fs pulse at a wavelength of 800 nm through the cytometry lens was calculated as follows:

$$\tau_1 = \tau_0 \sqrt{1 + \sum_{m=1}^{\infty} \left(\frac{z_m}{L_{D,m}} \right)^2}$$

$$\tau_1 = 100 \sqrt{1 + \left(\frac{0.012}{0.08} + \frac{0.003}{0.027} + \frac{0.003}{0.027} + \frac{0.009}{0.08} + \frac{0.005}{0.08} + \frac{0.005}{0.08} + \frac{0.003915}{0.08} + \frac{0.0008}{0.08} + \frac{0.00194}{0.1} \right)^2}$$

$$\tau_1 = 121 fs$$

Appendix 3 – Off-axis lengths for 20x/0.75 NA Nikon lens

RAY 1			RAY 3		
Element	thickness (mm)	error (mm)	Element	thickness (mm)	error (mm)
1	2.1	0.056	1	2.38	0.056
2	5.16	0.056	2	4.99	0.056
3	1.42	0.056	3	1.53	0.056
4	7.03	0.056	4	6.74	0.056
5	1.64	0.056	5	1.76	0.056
6	6.97	0.056	6	6.75	0.056
7	1.25	0.056	7	1.36	0.056
8	3.51	0.056	8	3.35	0.056
9	5.38	0.056	9	5.29	0.056
10	8.95	0.056	10	8.95	0.056
RAY 2			RAY 4		
Element	thickness (mm)	error (mm)	Element	thickness (mm)	error (mm)
1	2.16	0.056	1	2.61	0.056
2	5.10	0.056	2	4.71	0.056
3	1.47	0.056	3	1.7	0.056
4	6.97	0.056	4	6.35	0.056
5	1.7	0.056	5	1.93	0.056
6	6.91	0.056	6	6.42	0.056
7	1.25	0.056	7	1.53	0.056
8	3.46	0.056	8	3.23	0.056
9	5.44	0.056	9	5.15	0.056
10	9.0	0.056	10	8.9	0.056

Table 10 - The thickness of each element through which each ray propagates, measured using ImageJ of a generic Nikon objective lens (20x 0.75NA).

Ray 1, 2, 3 and 4 correspond to the ray on axis, 1 mm off axis, 2mm off axis and 3 mm off axis respectively.

The error of 0.056 mm is the error in calibration and was measured as ± 1 pixel, which corresponded to 0.056 mm since there were 147 pixels in the 8.33mm scale bar shown on Figure 9.

Appendix 4 – Wavelength dependent TPA cross-sections for Fluorescein

Wavelength (nm)	TPA Cross Section (GM)[6]
691	16
700	19
720	19
740	30
760	36
780	37
800	36
820	29
840	13
860	8
880	11
900	16
920	26
940	21
960	15

Table 11 – Data of the two-photon cross section for Fluorescein obtained from [48]**. Fluorescein in H_20 (pH=13)**

Appendix 5 – Negative GVD introduced by a grating pair at different wavelengths

β2 with a line separation (lines/mm) of….				
Grating separation	300	600	900	1200
5mm	-5.98×10^{-4}	-3.2×10^{-3}	-1.47×10^{-2}	-3.98×10^{-1}
7mm	-8.38×10^{-4}	-4.5×10^{-3}	-2.06×10^{-2}	-5.57×10^{-1}
10mm	-1.20×10^{-3}	-6.48×10^{-3}	-2.94×10^{-2}	-7.96×10^{-1}
20mm	-2.39×10^{-3}	-1.3×10^{-2}	-5.88×10^{-2}	-1.59×10^{0}
25mm	-2.99×10^{-3}	-1.62×10^{-2}	-7.35×10^{-2}	-1.99×10^{0}
50mm	-5.98×10^{-3}	-3.24×10^{-2}	-1.47×10^{-1}	-3.98×10^{0}
75mm	-8.98×10^{-3}	-4.86×10^{-2}	-2.21×10^{-1}	-5.97×10^{0}
100mm	-1.20×10^{-2}	-6.48×10^{-2}	-2.94×10^{-1}	-7.96×10^{0}
200mm	-2.39×10^{-2}	-1.30×10^{-1}	-5.88×10^{-1}	-15.9×10^{0}

Table 12 – The effective GVD (ps^2/m) introduced by a pair of gratings with a combination of different input parameters at a wavelength of 700nm.

β2 with a line separation (lines/mm) of….				
Grating separation	300	600	900	1200
5mm	-7.36×10^{-4}	-3.98×10^{-3}	-1.81×10^{-2}	-4.90×10^{-1}
7mm	-1.03×10^{-3}	-5.58×10^{-3}	-2.53×10^{-2}	-6.85×10^{-1}
10mm	-1.47×10^{-3}	-7.97×10^{-3}	-3.62×10^{-2}	-9.79×10^{-1}
20mm	-2.94×10^{-3}	-1.59×10^{-2}	-7.24×10^{-2}	-1.96×10^{0}
25mm	-3.68×10^{-3}	-1.99×10^{-2}	-9.04×10^{-2}	-2.45×10^{0}
50mm	-7.36×10^{-3}	-3.98×10^{-2}	-1.81×10^{-1}	-4.9×10^{0}
75mm	-1.10×10^{-2}	-5.98×10^{-2}	-2.71×10^{-1}	-7.35×10^{0}
100mm	-1.47×10^{-2}	-7.97×10^{-2}	-3.62×10^{-1}	-9.79×10^{0}
200mm	-2.94×10^{-2}	-1.59×10^{-1}	-7.24×10^{-1}	-19.6×10^{0}

Table 13- The effective GVD (ps^2/m) introduced by a pair of gratings with a combination of different input parameters at a wavelength of 750nm.

β2 with a line separation (lines/mm) of….				
Grating separation	300	600	900	1200
5mm	-1.07×10^{-3}	-5.80×10^{-3}	-2.63×10^{-2}	-7.13×10^{-1}
7mm	-1.50×10^{-3}	-8.12×10^{-3}	-3.69×10^{-2}	-9.98×10^{-1}
10mm	-2.14×10^{-3}	-1.16×10^{-2}	-5.27×10^{-2}	-1.43×10^{0}
20mm	-4.29×10^{-3}	-2.32×10^{-2}	-1.05×10^{-1}	-2.85×10^{0}
25mm	-5.36×10^{-3}	-2.90×10^{-2}	-1.32×10^{-1}	-3.56×10^{0}
50mm	-1.07×10^{-2}	-5.80×10^{-2}	-2.63×10^{-1}	-7.13×10^{0}
75mm	-1.61×10^{-2}	-8.70×10^{-2}	-3.95×10^{-1}	-10.7×10^{0}
100mm	-2.14×10^{-2}	-1.16×10^{-1}	-5.27×10^{-1}	-14.3×10^{0}
200mm	-4.29×10^{-2}	-2.32×10^{-1}	-1.05×10^{0}	-28.5×10^{0}

Table 14 - The effective (ps^2/m) GVD introduced by a pair of gratings with a combination of different input parameters at a wavelength of 850nm.

β2 with a line separation (lines/mm) of….				
Grating separation	300	600	900	1200
5mm	-1.27×10^{-3}	-6.88×10^{-3}	-3.13×10^{-2}	-8.46×10^{-1}
7mm	-1.78×10^{-3}	-9.64×10^{-3}	-4.38×10^{-2}	-1.18×10^{0}
10mm	-2.54×10^{-3}	-1.38×10^{-2}	-6.25×10^{-2}	-1.69×10^{0}
20mm	-5.09×10^{-3}	-2.75×10^{-2}	-1.25×10^{-1}	-3.38×10^{0}
25mm	-6.36×10^{-3}	-3.44×10^{-2}	-1.56×10^{-1}	-4.23×10^{0}
50mm	-1.27×10^{-2}	-6.88×10^{-2}	-3.13×10^{-1}	-8.46×10^{0}
75mm	-1.91×10^{-2}	-1.03×10^{-1}	-4.69×10^{-1}	-12.7×10^{0}
100mm	-2.54×10^{-2}	-1.38×10^{-1}	-6.25×10^{-1}	-16.9×10^{0}
200mm	-5.09×10^{-2}	-2.75×10^{-1}	-1.25×10^{0}	-33.8×10^{0}

Table 15 - The effective GVD (ps^2/m) introduced by a pair of gratings with a combination of different input parameters at a wavelength of 900nm.